

Department of Physics, Chemistry and Biology

Master's Thesis

Search for Dark Matter in the Upgraded High Luminosity LHC at CERN

A study of mono-jet signals in phase II upgrade

Sven-Patrik Hallsjö

Thesis work performed at Stockholm University

Linköping, June 4, 2014

LITH-IFM-A-EX--14/2863--SE



Linköpings universitet
TEKNISKA HÖGSKOLAN

Department of Physics, Chemistry and Biology
Linköping University
SE-581 83 Linköping, Sweden

Search for Dark Matter in the Upgraded High Luminosity LHC at CERN

A study of mono-jet signals in phase II upgrade

Sven-Patrik Hallsjö

Thesis work performed at Stockholm University

Linköping, June 4, 2014

Supervisor: **Docent Christophe Clément**
 FYSIKUM Stockholm University
Professor Magnus Johansson
 IFM, Linköping University

Examiner: **Professor Magnus Johansson**
 IFM, Linköping University



Avdelning, Institution
Division, Department

Theoretical physics group
Department of Physics, Chemistry and Biology
SE-581 83 Linköping

Datum
Date

2014-06-04

Språk

Language

Svenska/Swedish

Engelska/English

Rapporttyp

Report category

Licentiatavhandling

Examensarbete

C-uppsats

D-uppsats

Övrig rapport

ISBN

—

ISRN

LITH-IFM-A-EX--14/2863--SE

Serietitel och serienummer

Title of series, numbering

ISSN

—

URL för elektronisk version

<http://urn.kb.se/resolve?urn=urn:nbn:se:liu:diva-XXXXXX>

Titel

Sökandet efter mörk materia i den uppgraderade hög luminositets LHC i CERN

Title

Search for Dark Matter in the Upgraded High Luminosity LHC at CERN

Undertitel

En studie om mono-jet signaler i ATLAS fas II

Subtitle

A study of mono-jet signals in phase II upgrade

Författare

Sven-Patrik Hallsjö

Author

Sammanfattning

Abstract

Disclaimer: Abstract not yet completed.

Something as an introduction:

The LHC at CERN is undergoing an upgrade to increase the center of mass energy for the colliding particles which means that new physical processes will be explored. One drawback of this is that it will be harder to isolate unique particle collisions since more and more collisions will occur simultaneously, so called pile-up.

One hope for the upgrade is that WIMP models of dark matter will be detected.

This thesis covers looking at effective operators which try to explain dark matter without adding new theories to the standard model or QFT.

Some results and a slight conclusion.

Nyckelord

Keywords

Disclaimer: This not yet completed., ATLAS, Beyond standard model physics, CERN, Dark matter, Elementary particle physics, High energy physics, something, this is in mythesis.sty

4 **Abstract**

5 **Disclaimer: Abstract not yet completed.**

6 Something as an introduction:

7 The LHC at CERN is undergoing an upgrade to increase the center of mass en-
8 ergy for the colliding particles which means that new physical processes will be
9 explored. One drawback of this is that it will be harder to isolate unique parti-
10 cle collisions since more and more collisions will occur simultaneously, so called
11 pile-up.

12 One hope for the upgrade is that WIMP models of dark matter will be detected.

13 This thesis covers looking at effective operators which try to explain dark matter
14 without adding new theories to the standard model or QFT.

15 Some results and a slight conclusion.

16 **Acknowledgments**

17 [REDACTED]

18 A big thank you to my family, fiancée and friends who have supported me through-
19 out my education. A warm thank you to my friend Joakim Skoog who altered
20 some of the images for me.

21 [REDACTED]

22 [REDACTED]

23 *Linköping, June 2014*
24 *Sven-Patrik Hallsjö*

Contents

Notation

1 Introduction

| | | |
|-------|--|----|
| 1.1 | Research goals | 2 |
| 1.2 | Theoretical Background | 3 |
| 1.2.1 | Quantum mechanics and quantum field theory | 3 |
| 1.2.2 | Nuclear, particle and subatomic particle physics | 4 |
| 1.2.3 | The standard model of particle physics | 4 |
| 1.2.4 | Dark matter | 5 |
| 1.2.5 | Effective field theory | 6 |
| 1.2.6 | Search for WIMPS | 8 |
| 1.3 | Experimental overview | 10 |
| 1.3.1 | LHC | 10 |
| 1.3.2 | ATLAS | 11 |
| 1.3.3 | Coordinate system | 12 |
| 1.3.4 | Reconstructing data | 12 |
| 1.3.5 | Pile-up | 13 |
| 1.3.6 | Mono-jet analysis | 13 |
| 1.3.7 | Phase II high luminosity upgrade | 14 |
| 1.3.8 | Monte Carlo simulation | 15 |

2 Validation of smearing functions

| | | |
|-------|--------------------------------------|----|
| 2.1 | Smearing functions | 18 |
| 2.1.1 | Electron and photon | 18 |
| 2.1.2 | Muon | 18 |
| 2.1.3 | Tau | 18 |
| 2.1.4 | Jets | 18 |
| 2.1.5 | Missing Transversal Energy | 18 |
| 2.2 | Validation | 20 |
| 2.2.1 | Method | 20 |
| 2.3 | Results | 21 |
| 2.3.1 | Electron and photon | 22 |
| 2.3.2 | Muon | 23 |

| | | | |
|-----|----------|---|-----------|
| 58 | 2.3.3 | Tau | 23 |
| 59 | 2.3.4 | Jets | 24 |
| 60 | 2.3.5 | Missing Transversal Energy | 25 |
| 61 | 2.4 | Expected results | 26 |
| 62 | 2.5 | Discussion | 28 |
| 63 | 2.5.1 | Smearing independent on pile-up | 28 |
| 64 | 2.5.2 | Comparison to expected results | 28 |
| 65 | 2.6 | Conclusion | 29 |
| 66 | 3 | Evaluating dark matter signals | 31 |
| 67 | 3.1 | Signal to background ratio | 32 |
| 68 | 3.1.1 | Signal Region | 32 |
| 69 | 3.1.2 | Weight | 32 |
| 70 | 3.1.3 | Verification of background normalization | 32 |
| 71 | 3.1.4 | Errors in data | 33 |
| 72 | 3.1.5 | Figure of merit | 33 |
| 73 | 3.1.6 | D5 operator models | 35 |
| 74 | 3.1.7 | Light vector mediator models | 35 |
| 75 | 3.2 | Signal region definitions | 36 |
| 76 | 3.2.1 | Signal regions | 36 |
| 77 | 3.2.2 | Verifying background data | 36 |
| 78 | 3.3 | Mitigating the effect of the high luminosity | 36 |
| 79 | 3.4 | Results | 37 |
| 80 | 3.4.1 | Verifying background data | 37 |
| 81 | 3.4.2 | Events | 37 |
| 82 | 3.4.3 | Limit on M^* | 39 |
| 83 | 3.4.4 | Limit on mediator mass | 40 |
| 84 | 3.5 | Discussion | 43 |
| 85 | 3.5.1 | Comparison to previous results | 43 |
| 86 | 3.5.2 | Effect of the high luminosity | 43 |
| 87 | 3.6 | Conclusion | 44 |
| 88 | 3.6.1 | Limit on M^* | 44 |
| 89 | 3.6.2 | Limit on mediator mass | 44 |
| 90 | 3.6.3 | Effect of the high luminosity | 44 |
| 91 | 4 | Results and Conclusions | 45 |
| 92 | 4.1 | Validation of smearing functions | 45 |
| 93 | 4.2 | Signal to background ratio | 46 |
| 94 | 4.2.1 | Limit on M^* | 46 |
| 95 | 4.2.2 | Limit on mediator mass | 46 |
| 96 | 4.3 | Other selection criteria and observables | 46 |
| 97 | 4.3.1 | Limit on M^* | 46 |
| 98 | 4.3.2 | Limit on mediator mass | 46 |
| 99 | 4.4 | Mitigating the effect of the high luminosity | 46 |
| 100 | 4.5 | Recommendations to mitigate the effect of the high luminosity | 46 |
| 101 | 4.6 | Suggestions for future research | 46 |

| | | |
|-----|---|-----------|
| 102 | A Datasets | 49 |
| 103 | A.1 Background processes | 49 |
| 104 | A.1.1 Validation | 49 |
| 105 | A.1.2 Background to signals | 49 |
| 106 | A.2 Signals | 50 |
| 107 | A.2.1 Qcut | 50 |
| 108 | A.2.2 D5 signal processes | 50 |
| 109 | A.2.3 Light vector mediator processes | 50 |
| 110 | Bibliography | 53 |

Notation

NOTATIONS

| Notation | Explanation |
|----------|--|
| barn(b) | $1 \text{ barn}(b) = 10^{-24} \text{ cm}^2$ |
| \oplus | $a \oplus b = \sqrt{a^2 + b^2}$, $a \oplus b \oplus c = \sqrt{a^2 + b^2 + c^2}$ |

ABBREVIATIONS

| Abbreviation | Expansion |
|--------------|--|
| ATLAS | A large Toroidal LHC ApparatuS |
| CERN | Organisation européenne pour la recherche nucléaire ¹ |
| CMS | Compact Muon Solenoid |
| CR | Control Region |
| LHC | Large Hadron Collider |
| MC | Monte Carlo |
| RMS | Root Mean Square |
| SM | the Standard Model of particle physics |
| SR | Signal Region |
| WIMP | Weakly Interacting Massive Particle |
| WIMPS | Weakly Interacting Massive ParticleS |
| QED | Quantum ElectroDynamics |
| QFT | Quantum Field Theory |
| QM | Quantum Mechanics |

¹Originally, Conseil Européen pour la Recherche Nucléaire

1

Introduction

117 Discrepancies in measurements of the rotations of galaxies indicate the presence
118 of a large amount of matter which interacts through gravity, though not elec-
119 tromagnetically making it invisible to our telescopes. This matter is commonly
120 referred to as dark matter. Since no known or hypothesised particle in the stan-
121 dard model of particle physics can be used as a candidate for dark matter, this
122 hints at the presence of new physics.

123 At the Organisation Européene pour la Recherche Nucléaire (CERN) focus now
124 lies to discover any evidence of so called weakly interacting massive particles
125 (WIMPS) which may be a candidate for dark matter. It is usually impossible to
126 detect any interaction of dark matter candidates on the subatomic scale, however
127 through looking at proposed interactions, searching for assumed decay channels
128 and by investigating what is invisible to the detectors by using momentum con-
129 servation it is hoped that signs will be found. Though to date, none have been
130 found.

131 Both experiments and current theories now show that higher energies are re-
132 quired at the LHC to be able to see any signs. This is why the LHC and all detectors
133 are undergoing a vast upgrade program [1]. In this thesis focus will be on the last
134 part of the upgrade due for completion in 2023, known as the high luminosity-
135 LHC phase II upgrade; and also on the ATLAS detector. The method used in this
136 thesis focuses on looking at data which emulate conditions at the upgraded LHC.

137 1.1 Research goals

138 This research took place at Stockholm University from January 7th until **when**?
139 During the research period the following tasks were set up and performed/answered:

- 140 • Implement a C++ programme that loops over the collisions inside the signal
141 and background datasets.
- 142 • For each collision retrieve the relevant observables (variables used to extract
143 the signal over the background) and apply "smearing functions" to emulate
144 the effect of the high luminosity on the observables.
- 145 • For both signal and background datasets, compare observables before and
146 after smearing. What observables are the least/most affected?
- 147 • Implement selection criteria that selects the signal collisions efficiently while
148 reduces significantly the background. In a first step the selection criteria
149 should be taken from existing studies.
- 150 • Selection criteria can be evaluated and compared with each other using a
151 figure of merit P , that measures the sensitivity of the experiment to the dark
152 matter signal. Calculate P for the given selection criteria before and after
153 smearing.
- 154 • What is the effect of the high luminosity (smearing) on the value of P ?
- 155 • Investigate other selection criteria and observables, to mitigate the effect of
156 high luminosity. Use P to rank different criteria after smearing.
- 157 • Conclude on the effect of the high luminosity on the sensitivity for dark matter
158 and possible ways to mitigate its effects using alternative observables
159 and selection criteria.

1.2 Theoretical Background

1.2.1 Quantum mechanics and quantum field theory

In the beginning of the 20th century, some physical phenomena could not be explained by classical physics, for example the ultra-violet disaster of any classical model of black-body radiation, and the photoelectric effect [2]. It was these phenomena that led to the formulation of quantum mechanics (QM), where energy transfer is quantized and particles can act as both waves and particles at the same time [3].

Combining QM with classical electromagnetism proved harder than expected, colliding a photon(em-field) and an electron (particle/wave) is quite tricky. This can be seen when trying to calculate the scattering between them both in a QM schema. One idea that came from this was to explain them both in the same framework, field theory. Also, trying to incorporate special relativity into QM suggested a field description where space-time is described using the metric formalism from differential geometry. The culmination of both of these problems is the first part of a Quantum field theory (QFT), Quantum electrodynamics (QED) which with incredible precision explains electromagnetic phenomena including effects from special relativity[4]. It is in this merging that antimatter was theorised, since it is a requirement for the theory to hold. After the discovery of antimatter, the theory was set in stone. Since this the theory has been altered somewhat to explain more and more experimental data. This is discussed more in subsection 1.2.2 and subsection 1.2.3.

To be able to calculate properties in QFT one uses the Lagrangian formalism [5], which gives a governing equation for the different physical processes. In general the Lagrangian used for the Standard model is quite complicated, one can thus focus on one of the different terms corresponding to a specific interaction. This can be done to calculate the so called cross-section for a process, which is related to the probability that that process will occur. A step to simplify the calculations is to use the so called Feynman diagrams, an example of which is given in figure 1.1.

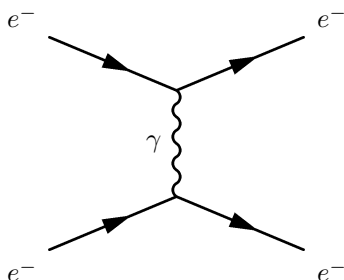


Figure 1.1: An example of a Feynman diagram explaining an electron-electron scattering using QED.

Through the figure, which comes with certain rules, and knowing what the major process (in this case QED) one can calculate the cross-section [4]. It is this that is needed to predict what one will be able to detect new particles.

1.2.2 Nuclear, particle and subatomic particle physics

Many could argue that these branches of physics started after Ernest Rutherford famous gold foil experiment [6], where he discovered that matter is composed of matter with a nucleus, a lot of empty space and electrons.

It was this that sparked the curiosity to see what the nucleus is made of and what forces govern the insides of atoms. After this, and the combination of the theoretical description given by QM, a lot more has been discovered and still more has been predicted. The newest of these is of course the Higgs particle, which was predicted through QFT and then discovered by the ATLAS and the CMS experiments at CERN [7].

The discovered particles are often divided into different groups depending on the fundamental particles that build them up. For instance, particles build up of three quarks are known as hadrons. Particles with an integer spin are known as bosons whereas half-integer particles are known as fermions.

1.2.3 The standard model of particle physics

The standard model of particle physics, referred to simply as the standard model (SM), is the particle zoo which tries to categorize all the particles and that have been discovered experimentally. QFT explains the interactions between these particles and it has also predicted several particles by including symmetries [6]. Regarding SM, Gauge bosons are the force carriers for the different forces, quarks are the and leptons are the fundamental blocks that we know of so far. The difference between the later two is if they interact via the strong force or not.

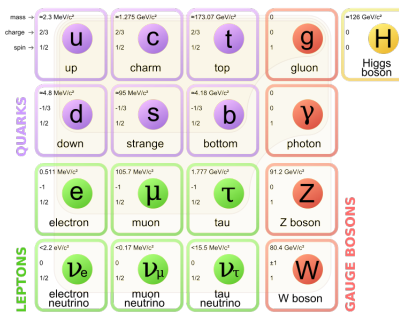


Figure 1.2: The standard model of particle physics where the three first columns represent the so called generations, starting with the first. [8].

SM is today the pinnacle of particle physics and can be used to explain almost everything that occurs around us. There are however some problems [9]:

- There is no link between gravity and the SM.
- Asymmetry between matter and antimatter can not be fully explained.
- No dark matter candidate!
- No explanation that can contain dark matter.

221 In this thesis focus lies with dark matter, some more introduction to possible
 222 dark matter and different candidates in extensions to SM are explained in subsection
 223 1.2.4.

224 1.2.4 Dark matter

225 Dark matter is among other things, the name given to the solution to the discrepancies
 226 of galactic rotations.

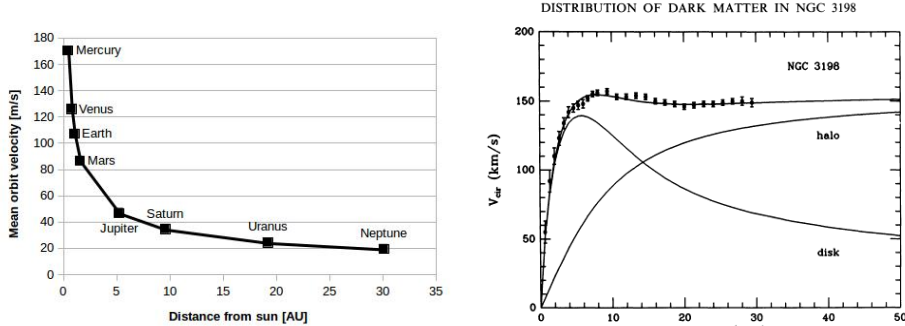
227 To explain this, focus on matter in a galaxy which are rotating around the center
 228 of the galaxy. Through Newtons law of gravity and the centrifugal force one can
 229 calculate the rotation speed dependent on the distance to the center of the galaxy.
 230 Since one of these forces is attractive and the other repulsive, if the matter is in
 231 a stable orbit around the galactic center (which they are) they must be equal and
 232 give us an expression for the speed depending on the distance. Newtons law can
 233 be written as the following:

$$F_{Gravitational} = G \frac{Mm}{r^2} = G_M \frac{m}{r^2} \quad F_{Centrifugal} = m \frac{V^2}{r} \quad (1.1)$$

234 where G is the gravitational constant, M the mass of the centre object, m the mass
 235 of the matter, r the distance between the two and V is the rotation speed. It has
 236 been simplified using G_M since all matter orbits the same galactic center. Setting
 237 the equations in (1.1) results in:

$$G_M \frac{m}{r^2} = m \frac{V^2}{r} \Leftrightarrow V^2 = \frac{G_M}{r} \Rightarrow V = \sqrt{\frac{G_M}{r}} \propto \frac{1}{\sqrt{r}} \quad (1.2)$$

238 where the speed is assumed to be positive and \propto means proportional. Through
 239 these simple calculations it shown that the rotation speed should decrease with
 240 and increased distance. The same reasoning can be applied to our solar system
 241 where this is the case figure 1.3a. The relation in these units is $V = \frac{107}{\sqrt{r}}$ where
 242 107 can be used in (1.2) to calculate the mass of the sun. However when looking
 243 at galaxies, even when taking into account that one has to see the galaxies as a
 244 mass distribution and that the above is only true when outside of the inner mass
 245 half, this is not the case! In figure 1.3b experimental data can be seen from the
 246 galaxy NGC3198 with a fitted curve which does not decrease with the distance
 247 but is instead constant. This is the discrepancy which is solved by postulating
 248 the existence of dark matter. After this the big question arises, what could this
 249 dark matter consist of? What is known so far lies in the name. It is called dark
 250 since there is no electromagnetic interaction and matter since it has gravitational
 251 interaction. This means that it can not be made up of any baryonic matter or
 252 anything in the Standard Model apart from neutrinos. The main interest of this
 253 thesis and also the main contributor to the rotational discrepancies is known as
 254 cold dark matter. This is due to the matter having a low speed, thus low kinetic
 255 energy, and have a high particle mass (In the GeV scale) [9, 12, 13]. This means
 256 however that neutrinos can not be a candidate, thus dark matter can not be made
 257 out of any standard model particles. There are several ideas to detected dark
 258 matter, [9]



(a) Rotation speed of planets in our solar system. Since the distance is quite small on an astronomical scale, there is no sign of dark matter. Based on data from [10].

(b) Rotation speed of matter in NGC3198 with a curve fitting and three different models, if only a dark model halo existed, if there was no dark matter and the correct, if both exist [11].

Figure 1.3: Different rotation curves, both for planets in our solar system and matter in the NGC3198 galaxy.

- Ordinary matter interacting with ordinary matter can produce dark matter, known as production. Which is the processes that occurs at particle accelerators.
- Dark matter interacting with ordinary matter can produce dark matter, known as direct detection.
- Dark matter interacting with dark matter can produce ordinary matter, known as indirect detection.

In this thesis the focus lies with production. There are several theories how to detect dark matter in proton-proton collisions such that occur at the LHC at CERN this is covered more in subsection 1.2.6.

1.2.5 Effective field theory

In quantum field theory the objective is usually to find the part of the Lagrangian which explains a type of interaction, known as the operator of the interaction and also to find the probability amplitude (cross-section) for a certain interaction. For complicated processes it is easier to employ certain conditions so that the small scale phenomena are simplified and the whole picture understood. This is known as using an effective field theory and the concept is explained in figure 1.4. The operator can be found through assuming the possible interactions and using the effective field theory [4]. The cross-sections can be found through the Feynman diagrams as described in subsection 1.2.1.

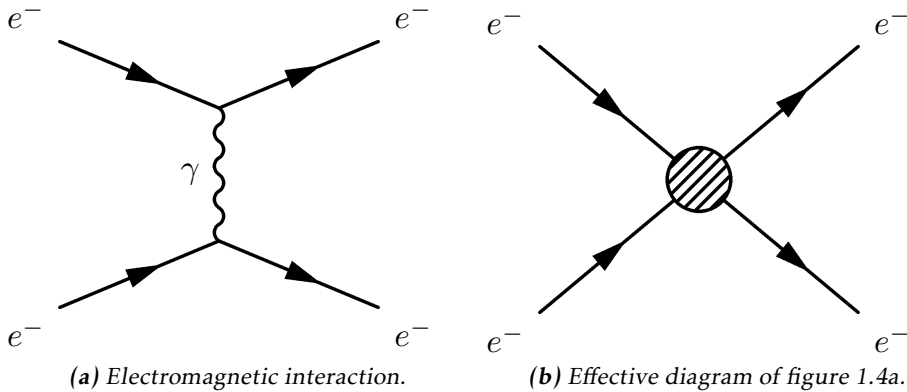


Figure 1.4: Feynman diagram of an electron-electron scattering, both as an ordinary diagram and as its effective theory version, where the details are hidden in the blob.

In this thesis the same effective field theory as in Refs. [12, 14] will be considered. The WIMP (usually denoted χ) is assumed to be the only particle in addition to the standard model fields. It is assumed that an even number of χ must be in every coupling. It is assumed that the mediator exists is heavier than the WIMPS, meaning that their interactions are in higher order terms of the effective field theory and thus not included in the operators. For simplicity, the WIMPS are assumed to be SM singlets, thus invariant under SM gauge transformations, and the coupling to the Higgs boson is neglected.

The operators used in this thesis are assumed to be quark bilinear operators on the form $\bar{q}\Gamma q$ where Γ is a 4×4 matrix of the complete set,

$$\Gamma = \{1, \gamma^5, \gamma^\mu, \gamma^\mu \gamma^5, \sigma^{\mu\nu}\} \quad (1.3)$$

This will dictate how the operators are written, more of why this is done can be found in [4, 12, 14].

This defines an effective field theory of the interaction of singlet WIMPs with hadronic matter. It is an approximation which will break down when the mediator mass is close to the mass of the WIMP. The condition for this is derived in [14] and gives:

$$M > 2m_\chi \quad (1.4)$$

where m_χ is the mass of the WIMP and M is the mass of the mediator particle. There is also the requirement that:

$$M \lesssim 4\pi M_* \quad (1.5)$$

where M_* is the energy scale where the effective theory is no longer a good approximation.

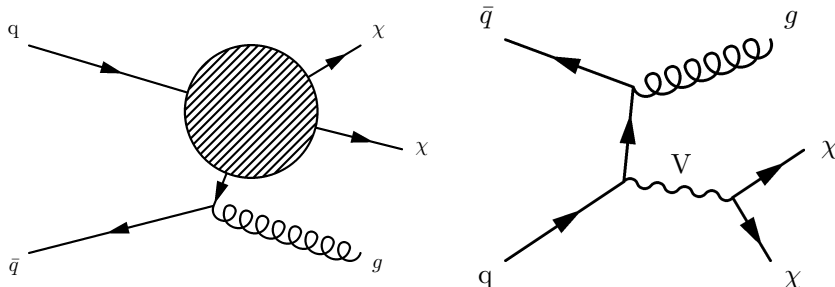
²⁹⁹ In this work, WIMPS are assumed to be Dirac fermions (half integer spin and is
³⁰⁰ not its own antiparticle).

³⁰¹ In table 1.1 the operators which are integrated out via the effective field theory
³⁰² and are of interest in this thesis are given.

| Name | Initial state | Type | Operator |
|------|---------------|--------------|---|
| D1 | qq | scalar | $\frac{m_q}{M_*^3} \bar{\chi} \chi \bar{q} q$ |
| D5 | qq | vector | $\frac{1}{M_*^2} \bar{\chi} \gamma^\mu \chi \bar{q} \gamma_\mu q$ |
| D8 | qq | axial-vector | $\frac{1}{M_*^2} \bar{\chi} \gamma^\mu \gamma^5 \chi \bar{q} \gamma_\mu \gamma^5 q$ |
| D9 | qq | tensor | $\frac{1}{M_*^2} \bar{\chi} \sigma^{\mu\nu} \chi \bar{q} \sigma_{\mu\nu} q$ |
| D11 | gg | scalar | $\frac{1}{4M_*^3} \bar{\chi} \chi \alpha_s (G_{\mu\nu}^a)^2$ |

Table 1.1: Table based on discussion in [13].

³⁰³ Where D denotes that the WIMPS are assumed to be Dirac fermions. These can all
³⁰⁴ be described using figure 1.5a.



(a) Effective Feynman diagram explaining the D-operators. **(b)** Feynman diagram describing the vector mediator model.

Figure 1.5: Feynman diagrams describing the signal models used in this thesis.

³⁰⁵ Another model which is considered is a vector mediator model which is described
³⁰⁶ by figure 1.5b.

1.2.6 Search for WIMPS

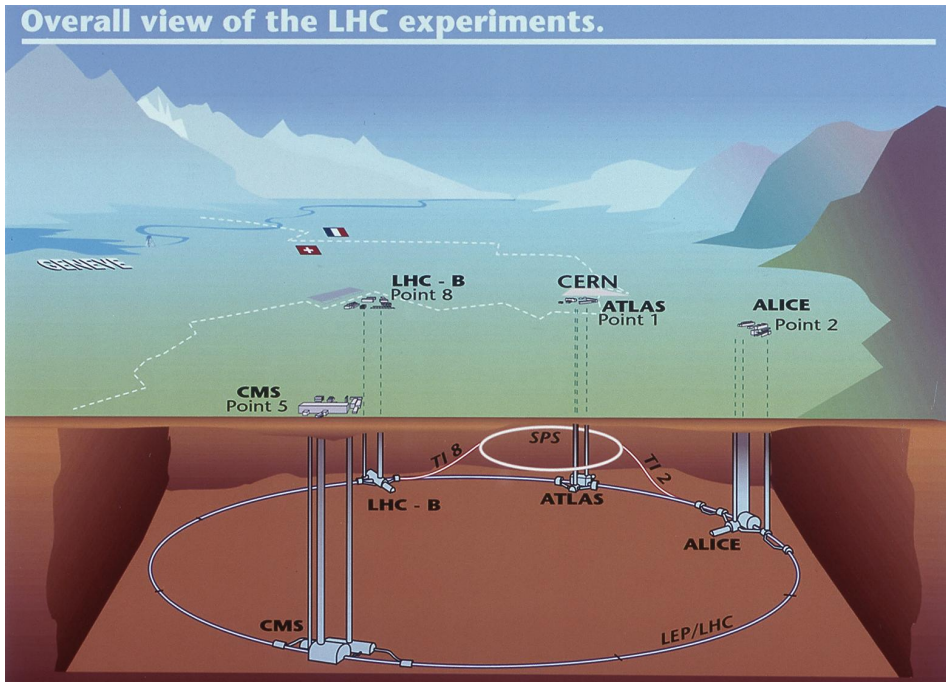
³⁰⁸ The search for WIMPS is based on a mono-jet analysis which is described in sub-
³⁰⁹ section 1.3.6. This method revolves around a high energetic jet which arises from
³¹⁰ the gluon from figure 1.5b and momentum missing from the energy conservation.

- 311 This means that something has happened which the detectors can not detect. If
312 the models from subsection 1.2.5 can explain the missing energy, then a model
313 for WIMPS has been found.
- 314 Since the search for WIMPS at the LHC is based on looking at the missing energy,
315 not actual detection, the experiment can not establish if a WIMP is stable on a
316 cosmological time scale and thus if it is a dark matter candidate [13]. This means
317 that if a candidate is found, it may still not be the dark matter that is needed to
318 explain the cosmological observations.
- 319 The different theories discussed in subsection 1.2.5 require some process in which
320 quarks and anti-quarks are produced. At ATLAS they have looked at proton-
321 proton collisions, in which they are produced, with 8 TeV center of mass energy
322 with out finding any excess of mono-jet events. This is why it is very interesting
323 that the LHC is undergoing a upgrade that will allow higher energy levels, see
324 subsection 1.3.7. With this the processes can be given higher energy and thus the
325 produced particles can be comprised of higher mass.

326 1.3 Experimental overview

327 1.3.1 LHC

328 The large hadron collider (LHC) is a particle accelerator located at CERN near
 329 Geneva in Switzerland, see figure 1.6. The accelerator was built to explore physics
 330 beyond the standard model and to make more accurate measurements of stan-
 331 dard model physics. Before it was shut down for an upgrade in 2012 it was able
 332 to accelerate two proton beams to such a velocity that each proton in them had
 333 an energy of 4 TeV which gives a center of mass energy, $\sqrt{s} = 8$ TeV. The proton
 334 beam is comprised of bunches of protons with enough spacing that bunch col-
 335 lisions can happen independent of each other. Apart from the energy, the rate at
 336 which the accelerator produces a certain process can be calculated through the
 337 instantaneous luminosity. For the LHC the instantaneous luminosity was 10^{34}
 338 $\text{cm}^{-2}\text{s}^{-1}$ [15] or $10\text{nb}^{-1}\text{s}^{-1}$ where 1 barn(b)= 10^{-24} cm^2 .



339 **Figure 1.6:** Figure showing the LHC and the different detector sites[16].

340 The instantaneous luminosity, often just denoted luminosity, can be defined in
 341 different ways depending on how the collision takes place. For two collinear
 intersecting particle beams it is defined as:

$$342 \mathcal{L} = \frac{f k N_1 N_2}{4\pi \sigma_x \sigma_y} \quad (1.6)$$

342 where N_i are the number of protons in each of the bunches, f is the frequency
 343 at which the bunches collide , k the number of colliding bunches in each beam,
 344 and σ_x (σ_y) is the horizontal (vertical) beam size at the interaction point. Since
 345 the instantaneous luminosity increases quadratically with more protons in each
 346 bunch, increasing the number of protons would be a good strategy to increase
 347 the instantaneous luminosity. However aside from the difficulties to create and
 348 maintain a beam with more particles, a large N_i increases the probability for
 349 multiple collisions per bunch crossing, referred to as pile-up. Pile up will be a
 350 key aspect which is described more in subsection 1.3.5.

351 The expected number of events can be calculated by using the instantaneous lu-
 352 minosity through the following:

$$N = \sigma \int \mathcal{L} dt \equiv \sigma \mathcal{L} \quad (1.7)$$

353 where \mathcal{L} is the integrated luminosity and σ is the cross section which is often
 354 measured in barn. The integrated luminosity is a measurement of total number
 355 of interactions that have occurred over time. Before the LHC was shut down \mathcal{L}
 356 was 20.8 fb^{-1} .

357 The cross section, as explained in subsection 1.2.1, is a measure of the effective
 358 surface area seen by the impinging particles, and as such is expressed in units
 359 of area. The cross section is proportional to the probability that an interaction
 360 will occur. It also provides a measure of the strength of the interaction between
 361 the scattered particle and the scattering center. Further details can be found in
 362 reference [17].

363 1.3.2 ATLAS

364 As seen in figure 1.6, there are several detectors at the LHC. One of these is
 365 ATLAS which is a general purpose detector that uses a toroid magnet. Its goal
 366 is to observe several different production and decay channels. The detector is
 367 composed of three concentric sub-detectors, the Inner detector, the Calorimeters
 368 and the Muon spectrometer [18].

369 The Inner detectors main task is to detect the tracks of the particles. It also mea-
 370 sures the position of the initial proton-proton collision.

371 The Calorimeters, electromagnetic and hadronic, are used to calculate the energy
 372 contained in the different particles. The electromagnetic detects particles which
 373 are charged, and the hadronic those which are neutral.

374 The Muon spectrometer is used to detect signs of muons, which will simply pass
 375 through the other detectors without leaving a trace. It also calculates the energy
 376 and momentum of the muons.

377 The neutrinos escape the ATLAS experiment without being detected, and in this
 378 thesis it is assumed that WIMPS pass through all the detectors without leaving
 379 any trace.

380 1.3.3 Coordinate system

381 The coordinate system of ATLAS, seen in figure 1.7 is a right-handed coordinate
 382 system with the x-axis pointing towards the centre of the LHC ring, and the z-axis
 383 along the tunnel/beam (counter clockwise) seen from above. The y-axis points up-
 384 ward. The origin is defined as the geometric center of the detector. A cylindrical
 385 coordinate system is also used for the transversal plane, (R, ϕ, Z) . For simplicity
 386 the pseudorapidity of particles from the primary vertex is defined as:

$$\eta = -\ln(\tan \frac{\theta}{2}) \quad (1.8)$$

387 where θ is the polar angle (xz-plane) of the particle direction measured from
 388 the positive z-axis. η is through this definition invariant under boosts in the z-
 389 direction.

390 It is quite common to calculate the distance between particles and jets in the
 391 (η, ϕ) space, $d = \sqrt{(\Delta\eta)^2 - (\Delta\phi)^2}$.

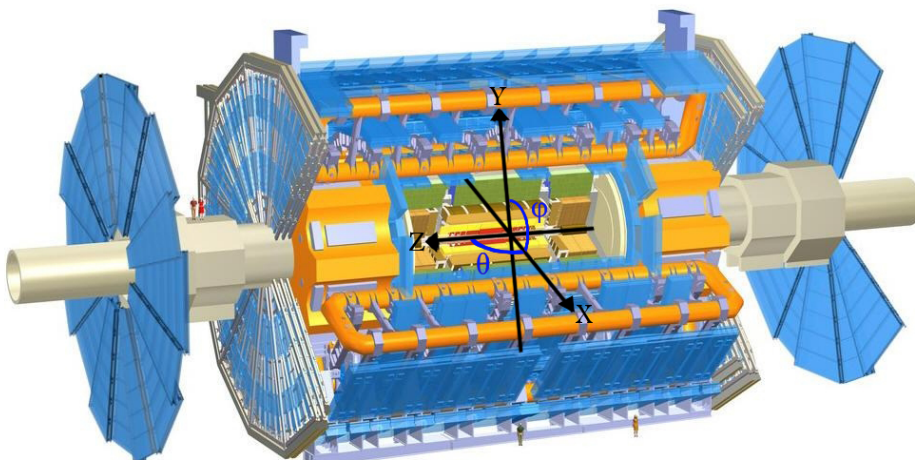


Figure 1.7: The ATLAS detector and the definition of the orthogonal Cartesian coordinate system. Image altered from[19]

392 1.3.4 Reconstructing data

393 To be able to compare the simulated data to real data it is important to include
 394 effects of the detectors. This is done using so called smearing functions which try
 395 to emulate the reconstruction of data.

396 The reconstruction process of data [18] is based on what response is given from
 397 the detectors. It is affected by pile-up and the energy of that which is detected.
 398 This process is not specifically used in the thesis, however the smearing functions
 399 are discussed in section 2.1.

400 1.3.5 Pile-up

401 Pile-up is the phenomena that several proton-proton collisions occur simultaneously.
 402 The number of pile-up is defined as the average number of proton-proton
 403 collisions that occur per bunch crossing per second. It is denoted as $\langle \mu \rangle$. μ can
 404 be calculated by adjusting a Poisson distribution to fit the curve created by the
 405 number of interactions per bunch crossing at a given luminosity. When this is
 406 done μ will be the mean value of the Poisson distribution.

407 1.3.6 Mono-jet analysis

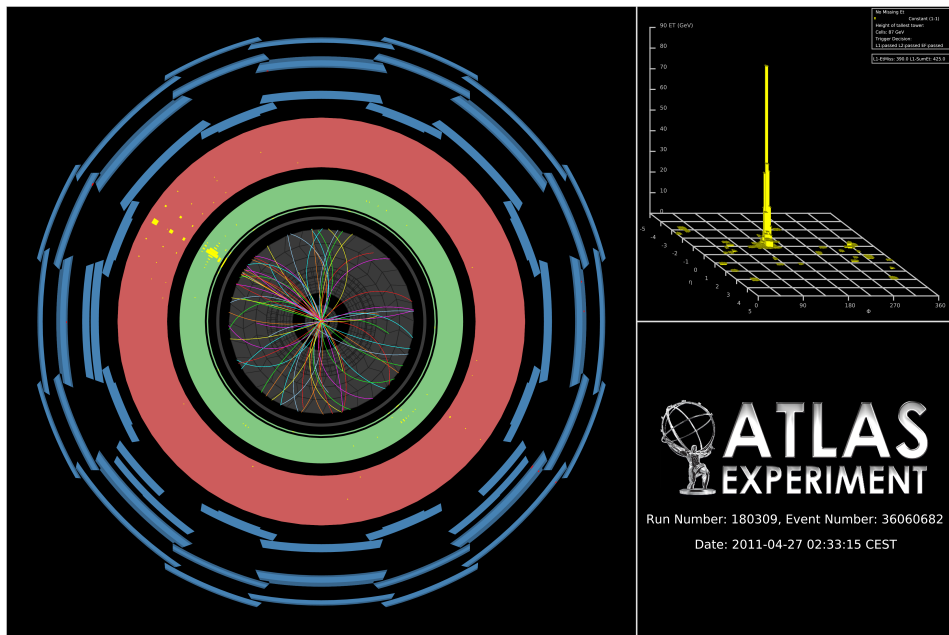


Figure 1.8: Image of an actual mono-jet event recorded by the ATLAS experiment [20].

408 When measuring the transversal energy one can in some interactions find incon-
 409 sistencies, such as jets that are in excess in one direction. In figure 1.8 one can see
 410 a high energetic jet which gives an excess of transversal energy in one direction
 411 after the collision. Since there is no balancing jet there must be transverse energy
 412 that is not detected, denoted E_T^{Miss} , since it was close to zero before the collision.
 413 This gives an indication that there energy to balance this that simply can not be
 414 detected. This could for instance be neutrinos or the sign of a new particle.

415 E_T^{Miss} is the modulus of the E_T^{Miss} vector which is defined as:

$$E_T^{\vec{M}iss} = -\sum E_T^{\vec{jet}} - \sum E_T^{\vec{Electron}} - \sum E_T^{\vec{\mu}on} - \sum E_T^{\vec{T}au} - \sum E_T^{\vec{\gamma}on} \quad (1.9)$$

416 Jets are hadrons which travel in the same direction and are usually created from

hadronization of a quark or a gluon in a collision. Usually jets are composed of a lot of energetic hadrons.

Since the jets are created from quarks or gluons, measuring a jet results in more information about the collision.

There are two main classes of events, signal and background. The signal corresponds to events that would arise from one of the processes in subsection 1.2.5. However to know that the missing energy is sign of the signal then one must understand all the other components that could contribute to the missing energy. Also there must be an excess of missing energy from what is expected from the background.

The background comprises of standard model processes that can mimic the mono-jet signature.

1.3.7 Phase II high luminosity upgrade

At the moment, the whole LHC is undergoing a step by step upgrade program which will be finalized around 2022-2023, denoted the high luminosity upgrade, or HL-upgrade. The upgrade consists of different stages, meaning that the upgrade will halt for periods so that experiments can take place. In figure 1.9 one can see

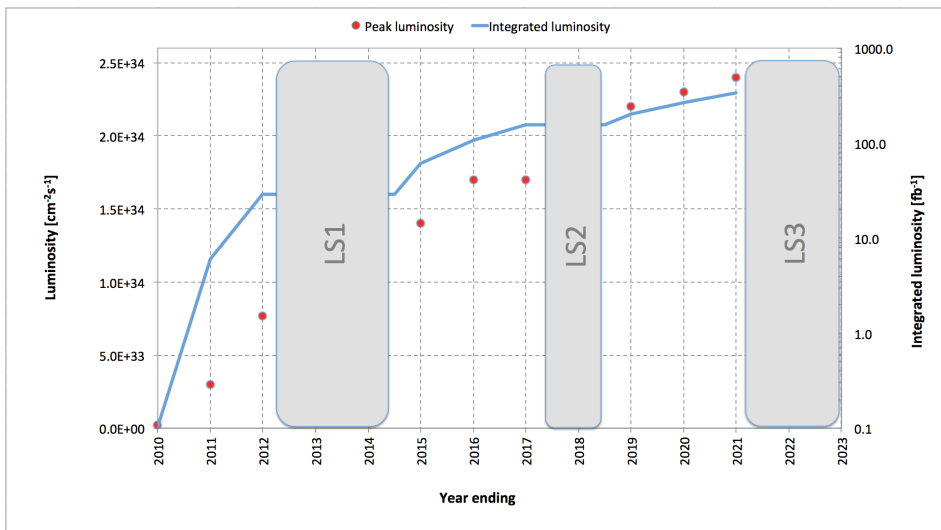


Figure 1.9: A graph showing the upgrading timetable with the instantaneous luminosity, denoted luminosity, and integrated luminosity expected in the different stages.

the three proposed upgrades. The period before LS1 is denoted phase 0, after LS1 and before LS2 phase I and after LS3 phase II.

LS1 is the upgrade which will take the LHC to its designed performance.

- 437 LS2 will take the LHC to the ultimate designed instantaneous luminosity.
 438 LS3 which is the focus of this thesis, will increase the instantaneous luminosity
 439 even more. Though for this to happen a modification of the whole LHC
 440 must be done, instead of just an upgrade and maintenance as before.

441 The following is expected for the experiments done after phase II:

| Entity | Expected | Last run (2012) |
|--------------------------|---|---|
| Instantaneous luminosity | $\mathcal{L} \sim 50 \text{ nb}^{-1} \text{s}^{-1}$ | $\mathcal{L} \sim 10 \text{ nb}^{-1} \text{s}^{-1}$ |
| Integrated luminosity | $\mathcal{L} = 1000 - 3000 \text{ fb}^{-1}$ | $\mathcal{L} = 20 \text{ fb}^{-1}$ |
| Pile-up | $\langle \mu \rangle = 140$ | $\langle \mu \rangle = 20$ |
| Center of mass energy | $\sqrt{s} = 14 \text{ TeV}$ | $\sqrt{s} = 8 \text{ TeV}$ |

Table 1.2: Expected running values for the Phase II HL-upgraded LHC with older values for comparison [21].

- 442 Where it should be noted that the integrated luminosity indicates the total amount
 443 of data which will be collected after the upgrade is completed before the next up-
 444 grade takes place.

445 1.3.8 Monte Carlo simulation

- 446 As mentioned before, in this thesis only emulated data has been used. This data
 447 is created by using a Monte Carlo (MC) simulation of the background processes
 448 and the expected signal. To do this a program called MadGraph is used.
 449 MadGraph [22] starts with Feynman diagrams and then generates simulated events
 450 based on lots of different parameters.
 451 PYTHIA [23] is a package which adds the correct description of jets to MadGraph
 452 by including hadronization. The correct description of pile-up comes from other
 453 ATLAS software.
 454 The tool to access all this data and analyse it a tool called ROOT, which is used
 455 for programming high energy physics related tools [24].

2

Validation of smearing functions

458 A full detector simulation of the ATLAS detector based on the GEANT [25] pro-
459 gram makes it possible to obtain the expected detector responses to electrons,
460 muons, tau leptons, photons (γ) and jets of hadrons. However these simulations
461 are extremely time-consuming and require a lot of computing power. Also at the
462 present time only a limited set of these simulations exists for the ATLAS phase II
463 upgrade.

464 In this thesis a different strategy is used. Instead of performing a full detector
465 simulation the observed particles from the event generator, which simulates the
466 proton-proton collisions, are smeared by using random numbers following reso-
467 lution functions specific to each type of particle. These emulate how the detector
468 and the reconstruction is affected by the increased luminosity and the pile-up
469 which comes with this.

470 The resolution functions or smearing functions are the official functions devel-
471 oped from previous studies [1, 26] by the ATLAS collaboration for the study of
472 the ATLAS phase II upgrade. The key feature of those studies was that the di-
473 rection of the momenta is unaffected and that only jets and E_T^{Miss} are affected by
474 pile-up. Since this was confirmed in previous studies it was not incorporated into
475 the smearing functions as discussed more in section 2.1.

476 Since part of this thesis work was to take the official ATLAS smearing functions
477 and apply the smearing to each particle, it was important to check that the en-
478 ergy and momenta resolutions of the smeared objects were consistent with the
479 expected values. Thus in this chapter the energy and momenta resolutions are
480 measured after applying the smearing to some simulated processes and the re-
481 sulting resolutions are compared with the expected values.

482 2.1 Smearing functions

483 These smearing functions are designed so that they take into account the effi-
484 ciency of the different detectors, limitations from how they are constructed as
485 well as their dependence on pile-up. They also take into account how all this
486 varies depending on the measured entries energy or momenta.

487 Terminology:

- 488 • Data before smearing, simulated data, is denoted as data at a truth level or
489 truth data.
- 490 • Data after smearing, which is comparable to what is measured is denoted
491 as reconstructed or reco data as discussed in subsection 1.3.4.

492 2.1.1 Electron and photon

493 The identification of electrons relies on finding an isolated electron track and
494 a pattern in the calorimeter compatible with an electron shower. Pile-up will
495 affect the electrons by decreasing the efficiency to identify an electron because of
496 the increased number of tracks. However for the identified electrons the energy
497 resolution will be close to that without pile-up.

498 The electron and photon have the same smearing since they are both detected in
499 a similar way.

500 2.1.2 Muon

501 The identification of muons relies on isolated tracks in the inner detector being
502 matched with information in the muon system. Since the muon system is the
503 outer most detector seen from the collision point it is unaffected by the false
504 detection effects of pile-up.

505 2.1.3 Tau

506 Tau is detected similarly to electron and photon. In this thesis all tau processes
507 are assumed to be at 3 prong. Where prong refers to the different amount of
508 tracks from which they were reconstructed. This in turn means that the effect of
509 pile-up will be worse compared to an electron as a triplet must be found in an
510 increased number of tracks.

511 2.1.4 Jets

512 The largest effect of pile-up is to add additional jets in the ATLAS detector. These
513 additional jets contribute to additional energy deposited inside the existing jets
514 and to E_T^{Miss} .

515 2.1.5 Missing Transversal Energy

516 E_T^{Miss} , the missing transversal energy, which was discussed in subsection 1.3.6,
517 and defined in (1.9) is calculated by knowing that there should be energy conser-

518 vation in the collision. It is comprised of different parts, one from neutrinos, one
519 from errors in the other measurements and one from new physics. It should be
520 affected by pile-up as described above.

521 2.2 Validation

522 To validate the smearing functions a comparison with Ref. [26] was made where
 523 the standard deviation, depending on the energy or momentum value of an entity,
 524 was given, see section 2.4. This is performed using the simulated processes listed
 in table 2.1.

Table 2.1: Different processes from where data has been taken. Each sample is a simulation of a physical process, the simulation names can be found in appendix A

| Particle | Process |
|---------------------|--|
| Electron | $W \rightarrow e\nu$ |
| Muon | $W \rightarrow \mu\nu$ |
| Tau | $W \rightarrow \tau\nu$ |
| γ | $\gamma + \text{Jet sample}$ |
| Jets | Jet sample |
| E_T^{Miss} | $Z \rightarrow \nu\nu + \text{Jet sample}$ |

525

526 2.2.1 Method

527 The energy and momentum resolutions are obtained for each type of particle by
 528 comparing the values before and after smearing.

529 This is done by looking at the reco data for a given slice at a truth energy or mo-
 530 mentum value. Since the smearing functions takes a lot into account the match
 531 will not be a fine line as seen in figure 2.3b.

532 By fitting a Gaussian curve to this data will then result in the standard deviation
 533 which is used in the validation. The standard deviation is also known as the
 534 resolution of the data and will be denoted σ .

535 This resolution is then compared to previous results, [26].

536 To get enough statistics enough data must be available for a given truth energy
 537 or momenta and the analysis must be specific enough to only look at a narrow
 538 enough interval around this point.

539 Step by step method

- 540 • Take a MC sample with a given particle, i.e electrons.
- 541 • Choose a slice of electron which have a truth energy of a given value (75
 542 GeV for electrons).
- 543 • Plot the smeared electron energy for this slice of truth energy. Given for
 544 electrons and photons in figure 2.1.
- 545 • For this distribution of smeared energy, fit a Gaussian distribution and cal-
 546 culate the sigma value of this Gaussian.
- 547 • Compare this sigma, which is the calculated resolution to the expected res-
 548 olution given from the smearing functions.

549 2.3 Results

- 550 As discussed above, the method was to plot the data against its smeared counter-
551 part and through this determine σ to see if it conforms to the expected values.
- 552 Only one energy value is shown for simplicity, though the comparison was done
553 for different energy values.
- 554 The average number of pile-up is fixed at 60 as a benchmark unless anything else
555 is stated.
- 556 As the comparison, figure 2.4, figure 2.1, figure 2.2 and figure 2.5 are divided
557 depending on the different η values.
- 558 All results are summarized in table 2.5.

559 2.3.1 Electron and photon

560 Since these interact very similarly in the detector, their smearing functions are
 561 identical. The slice value represents at which value of unsmeared energy or mo-
 562 mentum this smearing occurs.

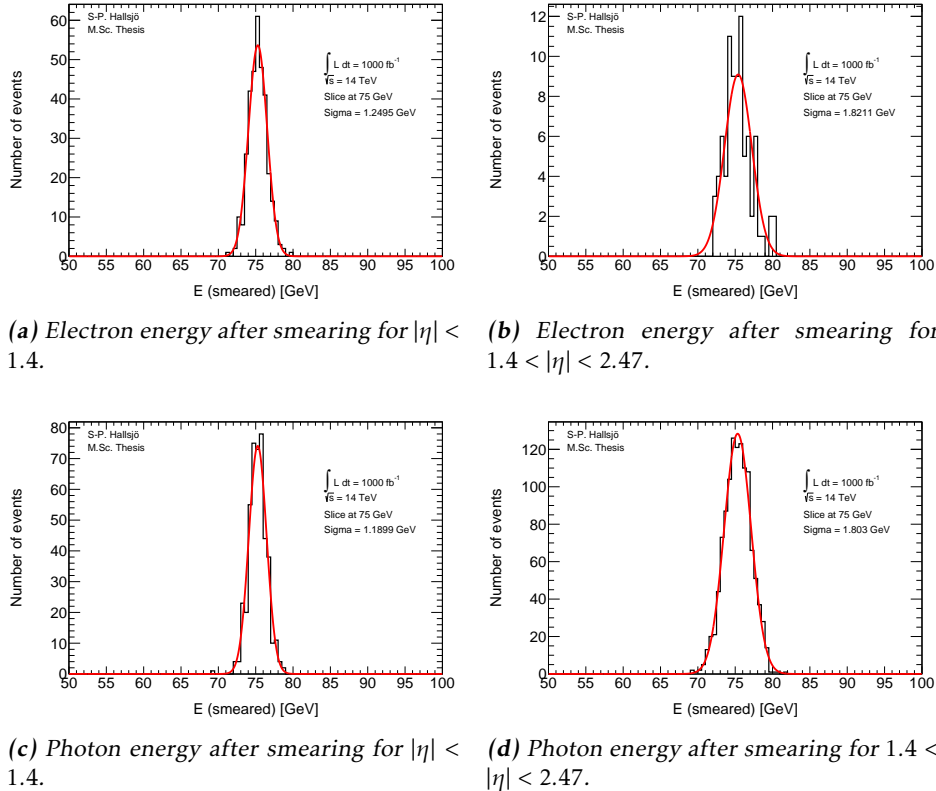
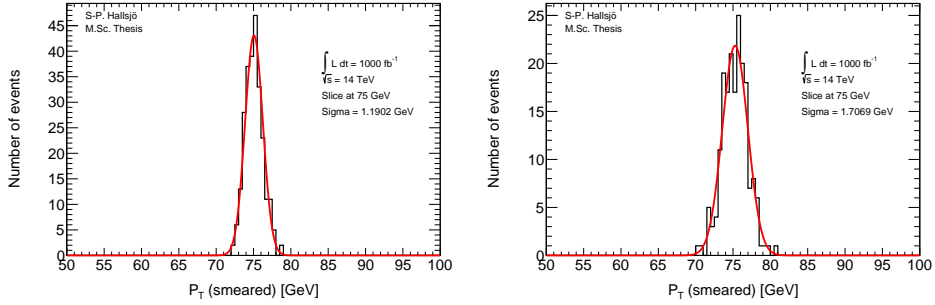


Figure 2.1: Photon and electron energy after smearing.

563 **2.3.2 Muon**

564 Since muons are shielded from the effects of pile-up only efficiency and detector
 565 limitations affect the smearing.

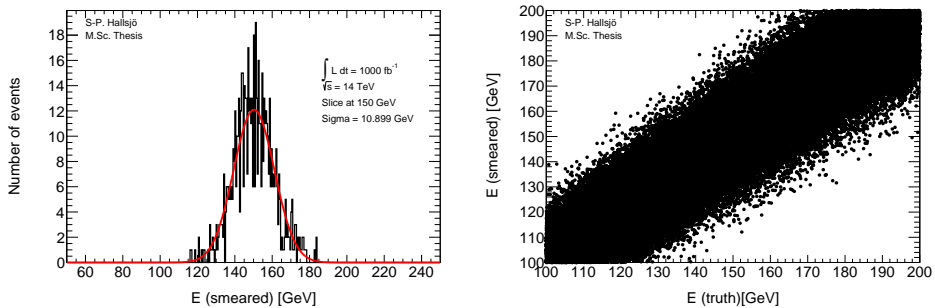


(a) Muon momenta after smearing for $|\eta| < 1.05$. (b) Muon momenta after smearing for $1.05 < |\eta|$.

Figure 2.2: Muon momenta after smearing.

566 **2.3.3 Tau**

567 As described in subsection 2.1.3 tauons are detected similarly to electrons and
 568 photons. Thus the plots should look similarly to those in the previous subsection
 569 apart from the slice being at 150 GeV. In figure 2.3a the Gaussian fit (red) and the
 570 data (black) are given for tau detected through 3 prong. In figure 2.3b smeared
 571 versus truth energy is shown.



(a) Tau energy after smearing.

(b) Tau energy vs smeared.

Figure 2.3: Tau energy after smearing and energy vs smearing.

2.3.4 Jets

Jets as described in subsection 1.3.6, are hadronic showers. The smearing functions are divided into four different regions depending on the angle η .

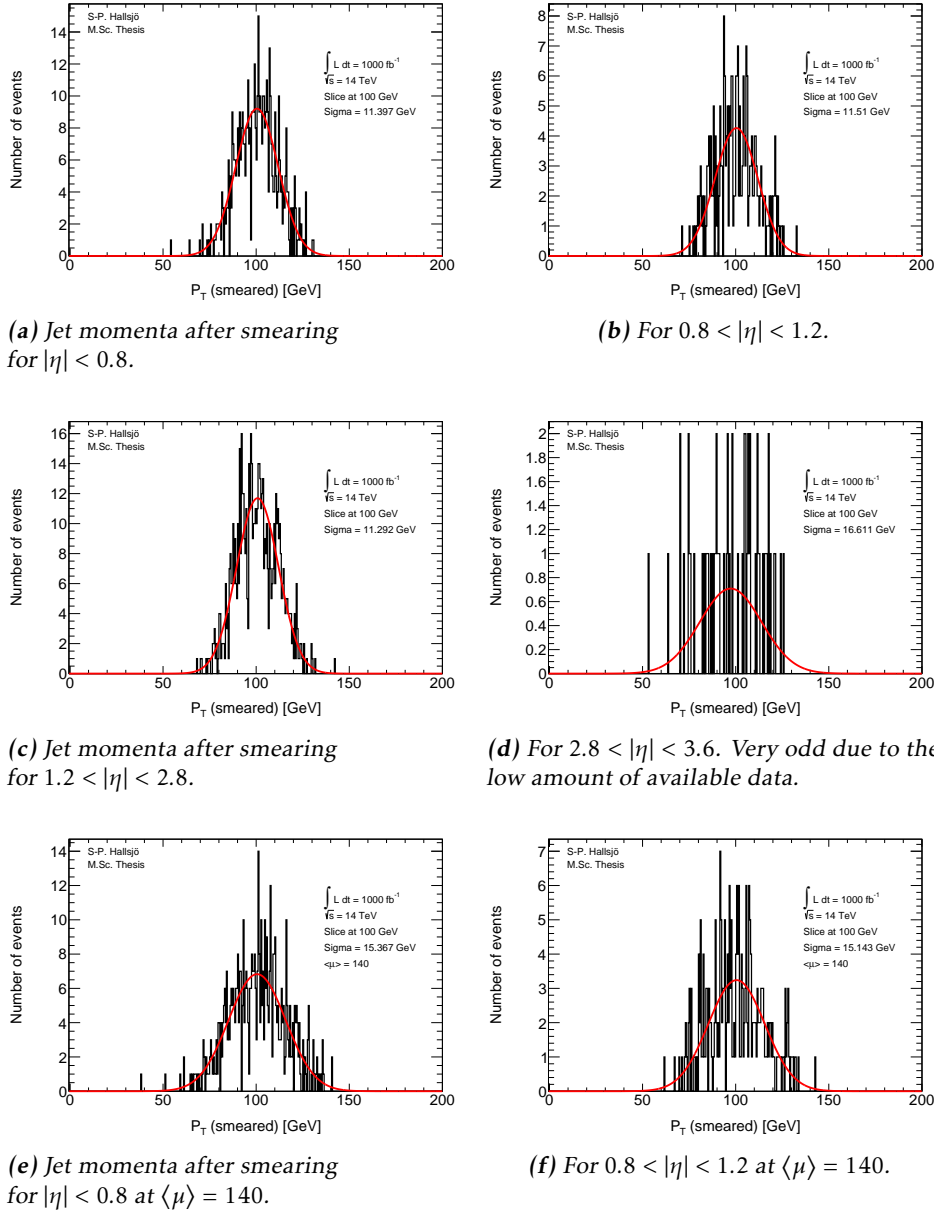


Figure 2.4: Jet momenta after smearing.

575 2.3.5 Missing Transversal Energy

576 The figures in this subsection are, compared to the above, given as absolute smear-
 577 ing, thus at 0 it represents that the energy is unsmeared, compared to the others
 578 where the slice value represents the unsmeared.

579 Here the E_T^{Miss} is projected down to the x- and y-axis, since these are the transver-
 580 sal axes, to be smeared.

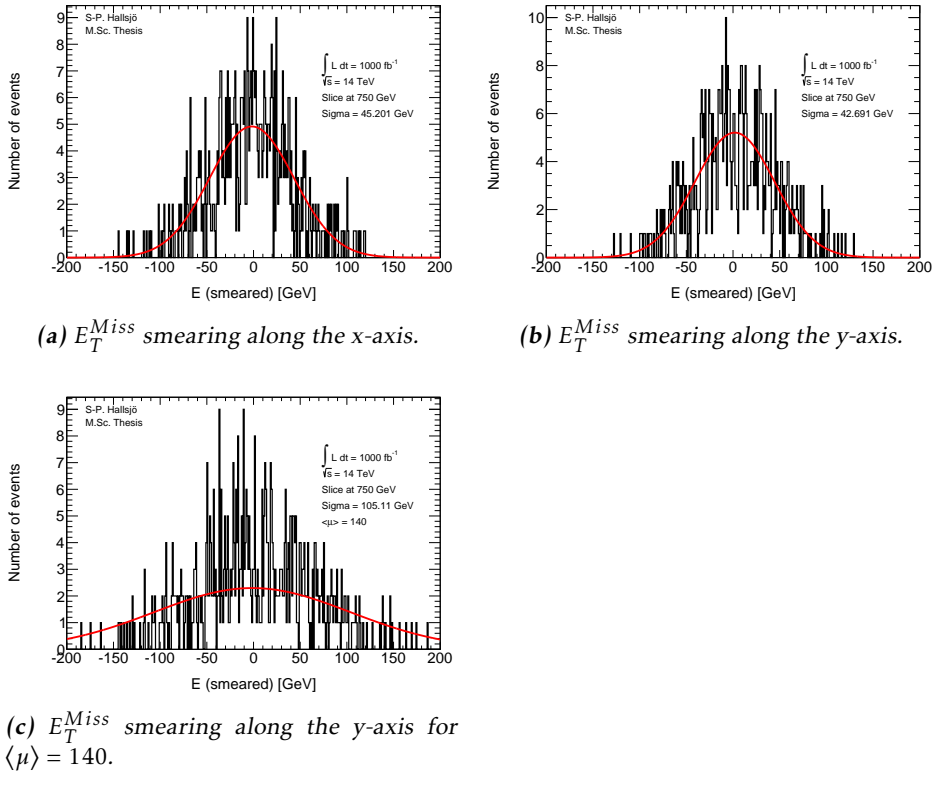


Figure 2.5: E_T^{Miss} smearing plots

581 2.4 Expected results

582 Since the leptons and photons are all detected by fitting detectors responses to
 583 different tracks, meaning that the effect of pile-up should be that there are more
 584 track to match, but it should not affect which ones are matched. The indepen-
 585 dence of pile-up for leptons and photons is backed up in previous research, for
 586 instance [1, 27].

587 To validate the smearing code, comparisons were made with [26] which gave the
 588 following formulation for the expected σ :

| Observable | Absolute σ |
|-------------------|---|
| Electron & photon | $\sigma = 0.3 \oplus 0.1\sqrt{E(GeV)} \oplus 0.01E(GeV), \eta < 1.4$ $\sigma = 0.3 \oplus 0.15\sqrt{E(GeV)} \oplus 0.015E(GeV), 1.4 < \eta < 2.47$ |
| Muon momentum | $\sigma = \frac{\sigma_{id}\sigma_{ms}}{\sigma_{id} \oplus \sigma_{ms}}$ $\sigma_{id} = P_T(a_1 \oplus a_2 P_T)$ $\sigma_{ms} = P_T(\frac{b_0}{P_T} \oplus b_1 \oplus b_2 P_T)$ |
| Tau energy | $\sigma = (0.03 \oplus \frac{0.76}{\sqrt{E(GeV)}})E(GeV), \text{for 3 prong.}$ |
| Jet momentum | $\sigma = P_T(GeV)(\frac{N}{P_T} \oplus \frac{S}{\sqrt{P_T}} \oplus C)$ where $N = a(\eta) + b(\eta)\mu$ |
| E_T^{Miss} | $\sigma = (0.4 + 0.09\sqrt{\mu})\sqrt{\sum E(GeV) + 20\mu}$ |

Table 2.2: Expected absolute σ where the parameters are given for muons in table 2.3 and for jets in table 2.4. Functions take from [26].

| | a_1 | a_2 | b_0 | b_1 | b_2 |
|-----------------|---------|----------|-------|---------|---------|
| $ \eta < 1.05$ | 0.01607 | 0.000307 | 0.24 | 0.02676 | 0.00012 |
| $ \eta > 1.05$ | 0.03000 | 0.000387 | 0.00 | 0.03880 | 0.00016 |

Table 2.3: Parameters used in the muon smearing function taken from [26].

| $ \eta $ | a | b | s | C |
|----------|-----|------|------|------|
| 0-0.8 | 3.2 | 0.07 | 0.74 | 0.05 |
| 0.8-1.2 | 3.0 | 0.07 | 0.81 | 0.05 |
| 1.2-2.8 | 3.3 | 0.08 | 0.54 | 0.05 |
| 2.8-3.6 | 2.8 | 0.11 | 0.83 | 0.05 |

Table 2.4: Parameters used in the jet smearing function taken from [26].

| Process | σ [GeV] | Expected σ |
|-----------------------------|--------------------|-------------------|
| Electron low η | 1.25 ± 0.05 | 1.18 |
| High η | 1.82 ± 0.14 | 1.74 |
| Photon low η | 1.19 ± 0.04 | 1.18 |
| High η | 1.80 ± 0.04 | 1.74 |
| Muon low η | 1.19 ± 0.05 | 1.50 |
| High η | 1.71 ± 0.09 | 2.18 |
| Tau | 10.90 ± 0.31 | 10.34 |
| Jet low η | 11.40 ± 0.35 | 11.60 |
| $\langle \mu \rangle = 140$ | 15.37 ± 0.47 | 15.77 |
| Mid low η | 11.51 ± 0.52 | 11.94 |
| $\langle \mu \rangle = 140$ | 15.14 ± 0.68 | 15.95 |
| Mid high η | 11.29 ± 0.31 | 10.94 |
| High η | 16.61 ± 1.53 | 13.50 |
| E_T^{Miss} x-axis | 45.20 ± 1.35 | 48.45 |
| E_T^{Miss} y-axis | 42.69 ± 2.28 | 48.45 |
| $\langle \mu \rangle = 140$ | 105.11 ± 12.24 | 87.28 |

Table 2.5: σ values.

- 589 • Where the given σ is still the absolute.
- 590 • Where the large difference between calculated and expected σ for Muons
591 and E_T^{Miss} is explained by incorrectly calculated errors in σ .

592 2.5 Discussion

593 2.5.1 Smearing independent on pile-up

594 From the validation done it was interesting to note that the smearing functions
595 were created from previous studies, [1, 27], which had shown that leptons and
596 photons are not affected by pile-up. This may seem incredible however it be-
597 comes quite logical when one understands how the detectors work. To be able to
598 detect particles the detectors must detect an excess of energy which comes from
599 a particle passing through. This should not be distorted by an increased pile-up.
600 The amount of particles passing through will of course increase, but the detec-
601 tions should be unaffected as well as the recreation of the events. However with
602 the same logic it makes sense that jets and E_T^{Miss} are quite affected since they
603 are combined of several parts, either hadronic particles or by all the transversal
604 missing energy.

605 Another interesting part is how the effect diminishes with and increasing energy.
606 As seen above, and through the the formula, for the high energies which were of
607 interest here the effect is minimal.

608 2.5.2 Comparison to expected results

609 One of the major problems in the comparison was to get the significance of the
610 Gaussian fit to be calculated correctly. The tool ROOT has a lot of different fea-
611 tures which made this task somewhat difficult. Also since this is a statistical
612 property there is a statistical fluctuation in the result.

613 Another was to retrieve the correct values from the paper, [26], since it was un-
614 clear if the values given were absolute or scale dependent. This has now been
615 corrected in a new version of the paper.

616 **2.6 Conclusion**

- 617 The smearing functions work as intended within 5.8 sigma, however when using
618 a test box and averaging the sigmas one ends up with half of this for the extreme
619 cases, muons and E_T^{Miss} y-axis.

620

3

621

Evaluating dark matter signals

622 **Disclaimer: All data provided is still a work in progress and may be subject to
623 change before the final version.**

624 The main goal of the thesis is to investigate if certain dark matter signals can
625 be detected after the high luminosity upgrade. One immediate worry is that the
626 background will be large in comparison to the signal, making the signal undetectable.
627

628 Another goal is to investigate if it might become more difficult to differentiate
629 between the signal and background due to the degradation of jet and missing
630 energy resolutions in the high luminosity upgrade.

631 This thesis focus on using a luminosity at 1000 fb^{-1} and a center of mass energy
632 at 14 TeV. The reco data is created using a pile-up rate, $\langle \mu \rangle = 140$ as expected
633 during phase II.

634 The signal models are given in appendix A along with the background models.
635 The different models were introduced subsection 1.2.5 and will be discussed in
636 more detail in this chapter.

637 Each signal model has been evaluated in different signal regions and the de-
638 tectability has been evaluated using a statistical P-value. This process has been
639 performed at a pile-up value of 140, as expected for after the high luminosity
640 upgrade.

641 3.1 Signal to background ratio

642 3.1.1 Signal Region

643 A signal region (SR) is defined as a set of selections on event variables designed
 644 to create a sample which is enriched in signal and depleted of background. One
 645 usually tries to design the signal region so that the signal is large enough and the
 646 background small enough that one would statistically be able to either:

- 647 • Exclude the signal if the observation of the data is compatible with a back-
 ground only hypothesis.
- 649 • Detect the signal and quantify the significance of the excess in data over
 650 background if the data is consistent with a signal + background hypothesis.

651 An event is a recorded proton-proton collision which consists of hundreds or
 652 thousands of observables such as the number of electrons, muons, jets, tau leptons,
 653 gammas or E_T^{Miss} each with their energy and momenta.

654 To define an optimal signal region is not known a priori and has to be studied for
 655 different signal models. The optimal region typically changes e.g with a change
 656 of the mass of new particles for instance the WIMP mass or the suppression scale.
 657 This is why there are several different signal regions to be studied in this thesis.

658 3.1.2 Weight

659 A weight is used to normalize different types of data so that they can be compared.
 660 As given in (1.7), the total number of events can be estimated as:

$$N = \sigma \int \mathcal{L} dt \equiv \sigma \mathcal{L} \quad (3.1)$$

661 Thus, if all events are generated at different luminosities, depending on the com-
 662 puting power of the computer which performed the simulation, the following
 663 weight should be used to receive the events at a new luminosity:

$$weight = \frac{\mathcal{L}\sigma}{N_{Raw}} \quad (3.2)$$

664 where N_{Raw} is the number of events expected at the luminosity that was set to cre-
 665 ate the data, compared to \mathcal{L} which is the luminosity at which the data is compared
 666 and σ is the cross-section. In this thesis the luminosity is fixed at $\mathcal{L} = 1000\text{fb}^{-1}$.

667 3.1.3 Verification of background normalization

668 To verify that the background samples are correctly normalized they are com-
 669 pared with Ref. [28] in which the center of mass energy is 8 TeV and the lumi-
 670 nosity is 10 fb^{-1} . Since the luminosity is not 1000 fb^{-1} as used in this thesis the
 671 expected values from the paper scaled up with a factor 100 to be comparable.

672 Somewhat unexpectedly a center of mass energy at 8 TeV had cross-sections a fac-
 673 tor 4 lower than the cross-sections at 14 TeV. These cross-sections are generated

either with MadGraph[22] or PYTHIA[23] depending on the generator given for each dataset in appendix A.

The signal regions used in the article were the following:

| Selection Criteria | | |
|---|------|------|
| Jet veto, require no more than 2 jets with $p_T > 30\text{GeV}$ and $ \eta < 4.5$ | | |
| Lepton veto, no electron or muon | | |
| Leading jet with $ \eta < 2.0$ and $\Delta\phi(\text{jet}, E_T^{Miss}) > 0.5$ (second-leading jet) | | |
| signal region | SR3p | SR4p |
| minimum leading jet p_T (GeV) | 350 | 500 |
| minimum E_T^{Miss} (GeV) | 350 | 500 |

Table 3.1: The signal regions from Ref. [28].

The article [28] has in total four signal regions, unfortunately since the simulated events used in this thesis are filtered before the analysis only the two highest regions are comparable. This can be seen in table 3.3 in subsection 3.4.1.

3.1.4 Errors in data

To make a thorough analysis of the background it is important to take into consideration different errors that exist in the number of events. This is especially important when looking at which signals can be excluded in different signal regions. There exists three main types of errors:

- Statistical errors from MC.
- Statistical errors from the control region.
- Systematic errors.

The statistical errors from MC come from the method of generating background events and is unfortunately nothing that can be estimated when one is not generating the events.

The statistical errors from the control region require an explanation of what a control region is. A control region (CR) is similar to a signal region, a set of criteria which are imposed on the data. This criteria are not set so that there can be a region with almost no signal. In this CR there will still be fluctuations in the amount of background events due to statistical effects, which can then be measured.

The systematic errors is a fixed error which is always present coming from different approximations in how all the events were generated.

3.1.5 Figure of merit

To be able to evaluate different signal regions and different signal models, a figure of merit p is used. The value p is the probability for the background to fluctuate

to the value of the signal + background. Thus if the p-value is small, regardless if the signal is large or the background or its fluctuations are small, it is improbable that the background could result in the same value as if there was a signal and background. This means that for a sufficiently small p-value the signal is detectable.

Assuming the expected number of background events are $B \pm \sigma_B$ where σ_B is the quadratic sum of the statistical error from Monte Carlo, the statistical error from the control region (CR) and the systematic errors as explained in subsection 3.1.5. The expected number of signal events is S , assumed without fluctuation.

If no uncertainty in B or S is assumed, then the probability that the background will fluctuate up to the signal and background should follow a Poisson distribution as such:

$$P(S+B|B) = \frac{e^{-B} B^{(S+B)}}{(S+B)!} \quad (3.3)$$

The probability that the background will fluctuate to a value N larger or equal to the signal and background then becomes:

$$P(B \geq S+B|B) \equiv P(N|B) = \sum_{N=S+B}^{\infty} \frac{e^{-B} B^N}{N!} \quad (3.4)$$

However since there is an uncertainty in the background, the probability distribution $P(N|B)$ must be convoluted with a Gaussian function:

$$G(N_B|B, \sigma_B) = \frac{1}{\sigma_B \sqrt{2\pi}} e^{-\frac{(N_B-B)^2}{2\sigma_B^2}} \quad (3.5)$$

where N_B is the expected number of background events. The convolution is done using N_B as B resulting in the total probability density function:

$$\begin{aligned} F(N|N_B, \sigma_B) &= P(N|B)*G(N_B|B, \sigma_B) = \\ &= \int_{-\infty}^{\infty} P(N|N_B - B) G(N_B|B, \sigma_B) dN_B \end{aligned} \quad (3.6)$$

Inserting the sum over N leads to the probability of the background fluctuation to signal and background being obtained as.

$$p = \sum_{N=S+B}^{\infty} \int_{-\infty}^{\infty} P(N|N_B - B) G(N_B|B, \sigma_B) dN_B \quad (3.7)$$

In this thesis, two different models of the error in the background σ_B are used. Both models are based on Ref. [28]. As described in the beginning of this subsection the error is calculated as:

$$\sigma_B = \text{Statistical error from MC} \oplus \text{Statistical error in CR} \oplus \text{Systematic error}$$

- The statistical error from MC has been neglected since there is no way of estimating it.
- The statistical error from background CR has been taken from the article and assumed to decrease with the increased luminosity as, $\frac{30}{380} \frac{\sqrt{L_{old}}}{\sqrt{L_{new}}}$
- The systematic error has been given two different values, from the article: $\frac{30}{380}$ or fixed at 0.02.
- All this results the total error being used as either, 0.08 or 0.02.

3.1.6 D5 operator models

As described in subsection 1.2.5, one of the signals is modelled using the D5 operator. In this thesis two different scenarios are used, one at a dark matter mass of 50 GeV and one at 400 GeV.

Each of these models are modelled with a mass suppression scale, denoted M^* , which is connected to the cross-section of the process through:

$$\sigma_{new} = \frac{\sigma_{old}}{M^*} \quad (3.8)$$

In subsection 3.4.3 it is determined which values of M^* could be excluded with the upgraded LHC phase 2 upgrade and ATLAS.

3.1.7 Light vector mediator models

As described in subsection 1.2.5, the other signal model is a vector mediator model. In this thesis these signals have two different width scenarios and a number of different mediator mass scenarios. **Where width is related to the lifetime of the dark matter particle.** In addition to this there are, as with the D5 operator, two different dark matter masses, one at 50 GeV and one at 400 GeV.

The result of the investigation of which models are excludable with the upgraded LHC phase 2 upgrade and ATLAS are given in subsection 3.4.4.

3.2 Signal region definitions

3.2.1 Signal regions

To be able to compare signal results to previous papers new signal regions were devised. It was also discovered that the requirement of no electrons or muons was to harsh for the signal models. Because of this new signal criteria were devised.

| Selection Criteria | | | | | |
|--|-----|------|-----|------|------|
| Jet veto, require no more than 2 jets with $p_T > 30\text{GeV}$ and $ \eta < 4.5$ | | | | | |
| Lepton veto, no electron or muon. | | | | | |
| The electron veto is defined: $\Delta R(jet^{lead}, electron^{lead}) \geq 0.4$ and $electron^{lead} p_T > 20\text{GeV}$ removed. | | | | | |
| The muon veto is defined: $\Delta R(jet^{lead}, muon^{lead}) \geq 0.4$ and $muon^{lead} p_T > 20\text{GeV}$ removed. | | | | | |
| Leading jet with $ \eta < 2.0$ and $\Delta\phi(jet, E_T^{Miss}) > 0.5$ (second-leading jet) | SR1 | SR1p | SR2 | SR3 | SR4 |
| signal region | SR1 | SR1p | SR2 | SR3 | SR4 |
| minimum leading jet p_T (GeV) | 350 | 500 | 600 | 800 | 1000 |
| minimum E_T^{Miss} (GeV) | 350 | 500 | 600 | 800 | 1000 |
| signal region | SRa | SRb | SRc | SRd | |
| minimum leading jet p_T (GeV) | 350 | 350 | 350 | 350 | |
| minimum E_T^{Miss} (GeV) | 350 | 600 | 800 | 1000 | |

Table 3.2: The new signal regions

3.2.2 Verifying background data

To make sure that the altered electron veto still produces results comparable with [28] a comparison is made again. This can be seen in subsection 3.4.1 in table 3.4.

3.3 Mitigating the effect of the high luminosity

As discussed in subsection 2.5.1 the smearing functions effect of pile-up should be minimal in the high energy regions which are of interest in this thesis.

From the formulation of the smearing functions, the biggest effect should be seen at low energies. This is related to the difficulty for the hardware triggers to select events. This means that one drawback of the high luminosity upgrade is that very low energy signal regions will be lost.

The effect of the high luminosity is seen in chapter 3.4 and discussed in subsection 3.5.2.

760 3.4 Results

761 3.4.1 Verifying background data

762 In table 3.3 and table 3.4 a comparison has been made between the number of
 763 simulated background events at a truth level and the number of expected events
 764 by scaling up the values from Ref. [28] by a factor 100. Truth data was used to
 765 not let the increased pile-up value affect the comparison. It can be seen that the
 766 simulated events and expected events coincide quite well on all accounts apart
 767 from $W \rightarrow \tau\nu$, $W \rightarrow \mu\nu$ and thus the total as well.

768 The difference in $W \rightarrow \tau\nu$ can be explained by the fact that τ can not be recreated
 769 as a jet in the simulated events which it can in measured events.

770 The difference in $W \rightarrow \mu\nu$ is explained through the simulated events having a
 771 better separation of muons neutrinos and E_T^{Miss} .

| Process | SR3p | Expected SR3p | SR4p | Expected SR4p |
|-------------------------|--------|---------------|-------|---------------|
| $Z \rightarrow \nu\nu$ | 140298 | 152000 | 25250 | 27000 |
| $W \rightarrow \tau\nu$ | 40701 | 37000 | 5862 | 3900 |
| $W \rightarrow e\nu$ | 11229 | 11200 | 1507 | 1600 |
| $W \rightarrow \mu\nu$ | 13727 | 15800 | 1872 | 4200 |
| Total background | 205955 | 218000 | 34491 | 36700 |

Table 3.3: Comparison of the simulated and expected events from Ref. [28] with $\mathcal{L} = 1000\text{fb}^{-1}$, cross-sections corresponding to $\sqrt{s} = 8\text{TeV}$ and using the same electron veto.

| Process | SR1 | Expected SR1 | SR1p | Expected SR1p |
|-------------------------|--------|--------------|-------|---------------|
| $Z \rightarrow \nu\nu$ | 150753 | 152000 | 27569 | 27000 |
| $W \rightarrow \tau\nu$ | 49320 | 37000 | 7318 | 3900 |
| $W \rightarrow e\nu$ | 18329 | 11200 | 2534 | 1600 |
| $W \rightarrow \mu\nu$ | 22290 | 15800 | 3218 | 4200 |
| Total background | 240690 | 218000 | 40639 | 36700 |

Table 3.4: Comparison of the simulated and expected events from Ref. [28] with $\mathcal{L} = 1000\text{fb}^{-1}$, cross-sections corresponding to $\sqrt{s} = 8\text{TeV}$ and using a modified electron veto and muon veto.

772 3.4.2 Events

773 In the following tables the number of events are given using one of the D5 opera-
 774 tors as the signal, and the background in the different signal regions. The number
 775 of background events is also used for the vector mediator signals.

| Process at $\sqrt{s} = 14\text{TeV}$ | SR1 | SR2 | SR3 | SR4 | SRa | Srb | Src | Srd |
|--------------------------------------|--------|-------|-------|------|--------|-------|-------|------|
| D5, mDm=50 GeV, M*=1TeV | 129863 | 30219 | 10750 | 4391 | 129863 | 36410 | 12927 | 5221 |
| Z $\rightarrow \nu\nu$ | 604479 | 42657 | 8424 | 2111 | 604479 | 58614 | 11383 | 2843 |
| W $\rightarrow \tau\nu$ | 154140 | 7807 | 1308 | 295 | 154140 | 10679 | 1788 | 386 |
| W $\rightarrow e\nu$ | 61772 | 2890 | 485 | 110 | 61772 | 3961 | 654 | 152 |
| W $\rightarrow \mu\nu$ | 49114 | 2357 | 379 | 91 | 49114 | 3052 | 499 | 108 |
| Total background | 869505 | 55711 | 10597 | 2607 | 869505 | 76305 | 14325 | 3489 |

Table 3.5: Signal and background events for truth data in the signal regions.

| Process at $\sqrt{s} = 14\text{TeV}$ | SR1 | SR2 | SR3 | SR4 | SRa | Srb | SRc | Srd |
|--------------------------------------|--------|-------|------|------|--------|-------|-------|------|
| D5, mDm=50 Gev, M*=1TeV | 120295 | 28019 | 9978 | 4130 | 120295 | 38762 | 13752 | 5505 |
| Z $\rightarrow \nu\nu$ | 553735 | 39105 | 7681 | 1932 | 553735 | 71613 | 13145 | 3140 |
| W $\rightarrow \tau\nu$ | 156023 | 7741 | 1282 | 276 | 156023 | 14500 | 2174 | 467 |
| W $\rightarrow e\nu$ | 58874 | 2706 | 448 | 106 | 58874 | 5177 | 790 | 176 |
| W $\rightarrow \mu\nu$ | 47801 | 2299 | 380 | 89 | 47801 | 4031 | 618 | 139 |
| Total background | 816433 | 51850 | 9791 | 2404 | 816433 | 95322 | 16727 | 3922 |

Table 3.6: Signal and background events for reco data with $\langle \mu \rangle = 140$ in the signal regions.

776 **3.4.3 Limit on M^***

777 For the D5 operators as described in subsection 3.1.6 limits on the mass suppression
 778 has been calculated by evaluating at which point the signal is covered by
 779 the background, meaning that the p-value > 0.05 . This is done using the two
 780 different error models as described in subsection 3.1.5 as figures of merit.

781 The limit is found, seen as a horizontal line in both figure 3.1 and figure 3.2, when
 782 the p-value = 0.05. **Will insert new images**

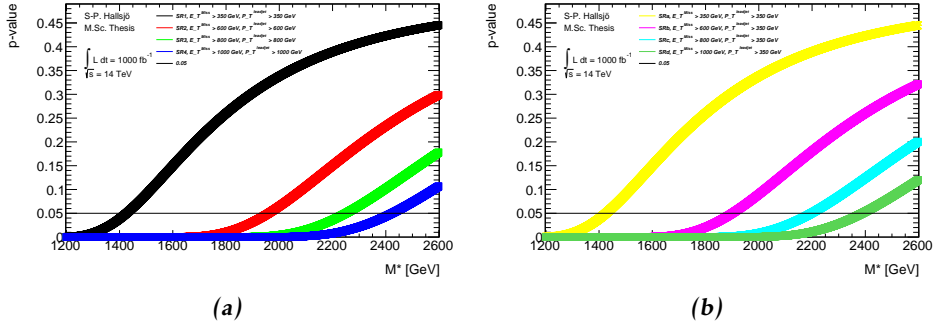


Figure 3.1: Limits of the mass suppression on a truth level for error model 0.02.

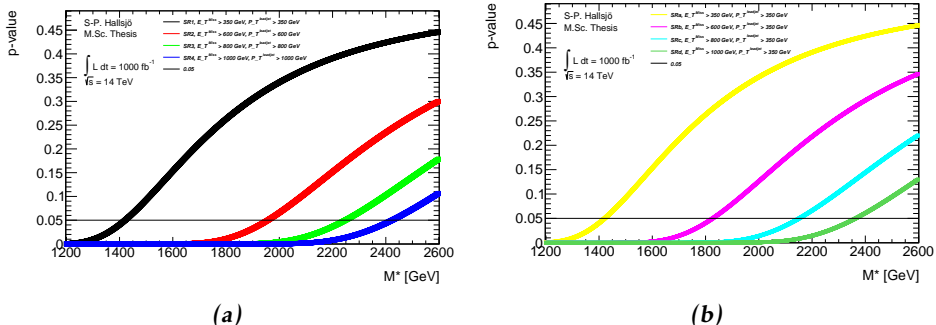


Figure 3.2: Limits of the mass suppression on a reco level for error model 0.02.

783 Calculating the intersection between these lines and 0.05 results in, tables 3.7-
 784 3.10 for both a dark matter mass of 50 GeV and at 400 GeV at the different error
 785 models.

| Signal region | Truth [GeV] | Reco [GeV] |
|---------------------|-------------|------------|
| SR1, symmetric 350 | 1425 | 1420 |
| SR2, 600 | 1960 | 1957 |
| SR3, 800 | 2249 | 2248 |
| SR4, 1000 | 2423 | 2423 |
| SRa, symmetric 350 | 1425 | 1421 |
| SRb, asymmetric 600 | 1900 | 1827 |
| SRc, 800 | 2197 | 2152 |
| SRd, 1000 | 2389 | 2363 |

Table 3.7: Limits on mass suppression scales in GeV given for $mDm=50$ GeV and the 0.02 error model.

| Signal region | Truth [GeV] | Reco [GeV] |
|---------------|-------------|------------|
| SR1 | 1015 | 1012 |
| SR2 | 1400 | 1400 |
| SR3 | 1636 | 1637 |
| SR4 | 1846 | 1854 |
| SRa | 1015 | 1012 |
| SRb | 1356 | 1303 |
| SRc | 1589 | 1553 |
| SRd | 1796 | 1768 |

Table 3.8: Limits on mass suppression scales in GeV given for $mDm=50$ GeV and the 0.08 error model.

786 3.4.4 Limit on mediator mass

787 For the vector mediator modes as described in subsection 3.1.7 limits on which
 788 models can be excluded have been calculated. This is done by calculating which
 789 models the p-value is < 0.05 . This is done using the two different error models as
 790 described in subsection 3.1.5 as figures of merit.

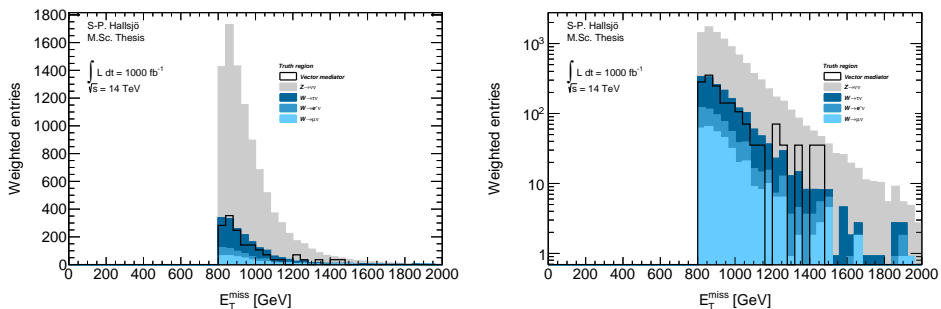
- 791 • Have a signal on background plot in a log scale just to show a trend.
- 792 • Add tables with the results.
- 793 • Write how this is done more in detail, with how these models are robust.
 794 **Do this again with new data.** See if they are still robust in truth vs reco
 795 and different error models.

| Signal region | Truth [GeV] | Reco [GeV] |
|---------------------|-------------|------------|
| SR1, symmetric 350 | 1350 | 1346 |
| SR2, 600 | 1871 | 1870 |
| SR3, 800 | 2185 | 2186 |
| SR4, 1000 | 2353 | 2322 |
| SRa, symmetric 350 | 1350 | 1346 |
| SRb, asymmetric 600 | 1814 | 1745 |
| SRc, 800 | 2134 | 2087 |
| SRd, 1000 | 2313 | 2281 |

Table 3.9: Limits on mass suppression scales in GeV given for $mDm=400$ GeV and the 0.02 error model.

| Signal region | Truth [GeV] | Reco [GeV] |
|---------------|-------------|------------|
| SR1 | 961 | 959 |
| SR2 | 1337 | 1337 |
| SR3 | 1589 | 1592 |
| SR4 | 1793 | 1777 |
| SRa | 961 | 959 |
| SRb | 1295 | 1245 |
| SRc | 1544 | 1507 |
| SRd | 1739 | 1707 |

Table 3.10: Limits on mass suppression scales in GeV given for $mDm=400$ GeV and the 0.08 error model.



(a) Signal on background plot for E_T^{Miss} on reco level in SR3.

(b) The same as a) with log scale on the y-axis

Figure 3.3: Signal on background plot to illustrate the a general plot. (OLD)

To set a limit on the mediator mass the p-value is calculated in different signal regions for the different signal models with different mediator mass. This resulted in the following plot.

- 799 The limit is found when the p-value = 0.05.
- 800 A table will be given with those models which survived in SR2 and SR3, and SR4
801 truth and reco.

802 3.5 Discussion

803 3.5.1 Comparison to previous results

804 Compared to 10fb paper ca 3-4 times better. Results was 800 GeV for mDM=50
805 GeV for my SR2 for 10fb-1 at 8TeV. I have: at 1000fb-1 and 14TeV.

806 Results was 700 GeV for mDM=400 GeV for my SR2 for 10fb-1 at 8TeV. I have:
807 at 1000fb-1 and 14TeV.

808 The whole discussion with Steven and David. **How should this be used? They**
809 **have no public results.**

810 Difference to the previous estimates may be explained by:

- 811 • Them using lower cross-sections for the background.
- 812 • The difference in treatment of CB.

813 3.5.2 Effect of the high luminosity

814 As seen in **Results**, the effect of a pile-up rate of 140 is minute in the signal
815 regions chosen. The primary focus of this thesis was to look at the effect of pile-
816 up, and try to mitigate the effect of it. However it is shown here that by choosing
817 signal regions with a high enough requirement the effect is minute. Thus the
818 focus was shifted to perform a more in-depth mono-jet analysis of different Dm
819 signal models. This modes were specifically the vector mediators.

820 Effect on m^*

821 As seen in the tables reference the ones in 3.4.3. above, comparing the truth
822 values against the reco values the difference is at most $< 5\%$. Thus these signal
823 regions are preferable for use in the high luminosity upgrade.

824 effect on mediator mass.

825 What is surprising is that if any model is viable in either truth or reco scenario
826 with any of the error-models, then it is viable for the rest.

827 Check the different cases for reco and truth to see what happens.

828 3.6 Conclusion

829 3.6.1 Limit on M^*

830 Give the limits from results.

831 3.6.2 Limit on mediator mass

832 Give the limits from results.

833 3.6.3 Effect of the high luminosity

834 At a pile-up level of 140 the effect is at most $< 5\%$ for the mass suppression scale
835 only affects vector mediator models which are borderline to survive as discussed
836 above. **Reference**.

837

4

838

Results and Conclusions

839 **Disclaimer: This chapter is not yet complete.**

840 4.1 Validation of smearing functions

841 Have some discussion.

842 Result they appear to work as expected, the reference paper was a bit unclear, I
843 leave my writing as a better reference.

4.2 Signal to background ratio844 **4.2.1 Limit on M***846 **4.2.2 Limit on mediator mass**847 **4.3 Other selection criteria and observables**848 **4.3.1 Limit on M***849 **4.3.2 Limit on mediator mass**850 **4.4 Mitigating the effect of the high luminosity**851 **4.5 Recommendations to mitigate the effect of the
852 high luminosity**

853 Keep to a higher energy region, or signal region.

854 **4.6 Suggestions for future research**

855 With more time, search for new signal regions, the only solution now for the HL
856 is to go up in energy. Since none of the other parameters (eta,phi etc) seem to be
857 altered these can not be used. Is there something that has been overlooked?

858 Test the effect of pile-up for lower signal regions? See if the effect is as great as
859 predicted.

860 Explore other theoretical models for dark matter, other d operators etc. Models
861 that are based on Supersymmetry and not just effective theories.

862 Sätt av ett kort kapitel sist i rapporten till att avrunda och föreslå räkningar för
863 framtida utveckling av arbetet.

864 Saving as reference. test citing as: Here we cite Duck [29] [29].

865 If the above works, remember to edit myreferences.

Appendix

867

A

868

Datasets

869 **Disclaimer: This appendix is not yet complete.**

870 **A.1 Background processes**

871 All datasets used are d4pd which is a dataformat used at CERN.

872 **A.1.1 Validation**

873 For the validation the following datasets were used, with a filter at generator level
874 at 450GeV for lead jet and MET.

875 157539 sherpa ct10 znunupt280 157534 sherpa ct10 wenupt200

876 157535 sherpa ct10 wmunupt200

877 157536 sherpa ct10 wtaunupt200

878 129160 pythia8 au2cteq6l1 perf jf17

879 129160 pythia8 au2cteq6l1 perf jf17

880 129170 pythia8 au2cteq6l1 gammajet dp17

881 They should be read as such: Monte Carlo version, dataset number, generator, ?
882 name.

883 **A.1.2 Background to signals**

884 The same as the above though now with the filter as indicated by their name. The
885 second znunu sample has been generated with and center of mass energy at 8
886 TeV.

887 157539 sherpa ct10 znunupt280

888 157539 8tev sherpa ct10 znunupt280

```

889 157536 sherpa ct10 wtaunupt200
890 157534 sherpa ct10 wenupt200
891 157535 sherpa ct10 wmunupt200

```

892 A.2 Signals

893 A.2.1 Qcut

894 Qcut means that the original data has been split into different parts depending
 895 on the value of the lead jet pt.

896 A.2.2 D5 signal processes

```

897 188408 madgraphpythia auet2bcteq6l1 d5 dm50 ms10000 qcut200
898 188409 madgraphpythia auet2bcteq6l1 d5 dm50 ms10000 qcut400
899 188410 madgraphpythia auet2bcteq6l1 d5 dm50 ms10000 qcut600
900 188411 madgraphpythia auet2bcteq6l1 d5 dm400 ms10000 qcut200
901 188412 madgraphpythia auet2bcteq6l1 d5 dm400 ms10000 qcut400
902 188413 madgraphpythia auet2bcteq6l1 d5 dm400 ms10000 qcut600

```

903 All signals should be read as such: Monte Carlo version, dataset number, generator, ?, name of operator, dark matter mass, default mass suppression scale,
 904 qcut part. As discussed in reference
 905

906 A.2.3 Light vector mediator processes

```

907 188414 madgraphpythia auet2bcteq6l1 dmv dm50 mm100 w3 qcut200
908 188422 madgraphpythia auet2bcteq6l1 dmv dm50 mm100 w3 qcut400
909 188430 madgraphpythia auet2bcteq6l1 dmv dm50 mm100 w3 qcut600
910 188415 madgraphpythia auet2bcteq6l1 dmv dm50 mm300 w3 qcut200
911 188423 madgraphpythia auet2bcteq6l1 dmv dm50 mm300 w3 qcut400
912 188431 madgraphpythia auet2bcteq6l1 dmv dm50 mm300 w3 qcut600
913 188416 madgraphpythia auet2bcteq6l1 dmv dm50 mm500 w3 qcut200
914 188424 madgraphpythia auet2bcteq6l1 dmv dm50 mm500 w3 qcut400
915 188432 madgraphpythia auet2bcteq6l1 dmv dm50 mm500 w3 qcut600
916 188417 madgraphpythia auet2bcteq6l1 dmv dm50 mm1000 w3 qcut200
917 188425 madgraphpythia auet2bcteq6l1 dmv dm50 mm1000 w3 qcut400
918 188433 madgraphpythia auet2bcteq6l1 dmv dm50 mm1000 w3 qcut600
919 188418 madgraphpythia auet2bcteq6l1 dmv dm50 mm3000 w3 qcut200
920 188426 madgraphpythia auet2bcteq6l1 dmv dm50 mm3000 w3 qcut400
921 188434 madgraphpythia auet2bcteq6l1 dmv dm50 mm3000 w3 qcut600
922 188419 madgraphpythia auet2bcteq6l1 dmv dm50 mm6000 w3 qcut200
923 188427 madgraphpythia auet2bcteq6l1 dmv dm50 mm6000 w3 qcut400
924 188435 madgraphpythia auet2bcteq6l1 dmv dm50 mm6000 w3 qcut600

```

```
925 188420 madgraphpythia auet2bcteq6l1 dmv dm50 mm10000 w3 qcut200
926 188428 madgraphpythia auet2bcteq6l1 dmv dm50 mm10000 w3 qcut400
927 188436 madgraphpythia auet2bcteq6l1 dmv dm50 mm10000 w3 qcut600
928 188421 madgraphpythia auet2bcteq6l1 dmv dm50 mm15000 w3 qcut200
929 188429 madgraphpythia auet2bcteq6l1 dmv dm50 mm15000 w3 qcut400
930 188437 madgraphpythia auet2bcteq6l1 dmv dm50 mm15000 w3 qcut600
931 188438 madgraphpythia auet2bcteq6l1 dmv dm50 mm100 w8pi qcut200
932 188446 madgraphpythia auet2bcteq6l1 dmv dm50 mm100 w8pi qcut400
933 188454 madgraphpythia auet2bcteq6l1 dmv dm50 mm100 w8pi qcut600
934 188439 madgraphpythia auet2bcteq6l1 dmv dm50 mm300 w8pi qcut200
935 188447 madgraphpythia auet2bcteq6l1 dmv dm50 mm300 w8pi qcut400
936 188455 madgraphpythia auet2bcteq6l1 dmv dm50 mm300 w8pi qcut600
937 188440 madgraphpythia auet2bcteq6l1 dmv dm50 mm500 w8pi qcut200
938 188448 madgraphpythia auet2bcteq6l1 dmv dm50 mm500 w8pi qcut400
939 188456 madgraphpythia auet2bcteq6l1 dmv dm50 mm500 w8pi qcut600
940 188441 madgraphpythia auet2bcteq6l1 dmv dm50 mm1000 w8pi qcut200
941 188449 madgraphpythia auet2bcteq6l1 dmv dm50 mm1000 w8pi qcut400
942 188457 madgraphpythia auet2bcteq6l1 dmv dm50 mm1000 w8pi qcut600
943 188442 madgraphpythia auet2bcteq6l1 dmv dm50 mm3000 w8pi qcut200
944 188450 madgraphpythia auet2bcteq6l1 dmv dm50 mm3000 w8pi qcut400
945 188458 madgraphpythia auet2bcteq6l1 dmv dm50 mm3000 w8pi qcut600
946 188444 madgraphpythia auet2bcteq6l1 dmv dm50 mm10000 w8pi qcut200
947 188452 madgraphpythia auet2bcteq6l1 dmv dm50 mm10000 w8pi qcut400
948 188460 madgraphpythia auet2bcteq6l1 dmv dm50 mm10000 w8pi qcut600
949 188445 madgraphpythia auet2bcteq6l1 dmv dm50 mm15000 w8pi qcut200
950 188453 madgraphpythia auet2bcteq6l1 dmv dm50 mm15000 w8pi qcut400
951 188461 madgraphpythia auet2bcteq6l1 dmv dm50 mm15000 w8pi qcut600
952 188462 madgraphpythia auet2bcteq6l1 dmv dm400 mm500 w3 qcut200
953 188468 madgraphpythia auet2bcteq6l1 dmv dm400 mm500 w3 qcut400
954 188474 madgraphpythia auet2bcteq6l1 dmv dm400 mm500 w3 qcut600
955 188463 madgraphpythia auet2bcteq6l1 dmv dm400 mm1000 w3 qcut200
956 188469 madgraphpythia auet2bcteq6l1 dmv dm400 mm1000 w3 qcut400
957 188475 madgraphpythia auet2bcteq6l1 dmv dm400 mm1000 w3 qcut600
958 188464 madgraphpythia auet2bcteq6l1 dmv dm400 mm3000 w3 qcut200
959 188470 madgraphpythia auet2bcteq6l1 dmv dm400 mm3000 w3 qcut400
960 188476 madgraphpythia auet2bcteq6l1 dmv dm400 mm3000 w3 qcut600
961 188465 madgraphpythia auet2bcteq6l1 dmv dm400 mm6000 w3 qcut200
962 188471 madgraphpythia auet2bcteq6l1 dmv dm400 mm6000 w3 qcut400
963 188477 madgraphpythia auet2bcteq6l1 dmv dm400 mm6000 w3 qcut600
```

964 188466 madgraphpythia auet2bcteq6l1 dmv dm400 mm10000 w3 qcut200
965 188472 madgraphpythia auet2bcteq6l1 dmv dm400 mm10000 w3 qcut400
966 188478 madgraphpythia auet2bcteq6l1 dmv dm400 mm10000 w3 qcut600
967 188467 madgraphpythia auet2bcteq6l1 dmv dm400 mm15000 w3 qcut200
968 188473 madgraphpythia auet2bcteq6l1 dmv dm400 mm15000 w3 qcut400
969 188479 madgraphpythia auet2bcteq6l1 dmv dm400 mm15000 w3 qcut600
970 188480 madgraphpythia auet2bcteq6l1 dmv dm400 mm500 w8pi qcut200
971 188486 madgraphpythia auet2bcteq6l1 dmv dm400 mm500 w8pi qcut400
972 188492 madgraphpythia auet2bcteq6l1 dmv dm400 mm500 w8pi qcut600
973 188481 madgraphpythia auet2bcteq6l1 dmv dm400 mm1000 w8pi qcut200
974 188487 madgraphpythia auet2bcteq6l1 dmv dm400 mm1000 w8pi qcut400
975 188493 madgraphpythia auet2bcteq6l1 dmv dm400 mm1000 w8pi qcut600
976 188482 madgraphpythia auet2bcteq6l1 dmv dm400 mm3000 w8pi qcut200
977 188488 madgraphpythia auet2bcteq6l1 dmv dm400 mm3000 w8pi qcut400
978 188494 madgraphpythia auet2bcteq6l1 dmv dm400 mm3000 w8pi qcut600
979 188483 madgraphpythia auet2bcteq6l1 dmv dm400 mm6000 w8pi qcut200
980 188489 madgraphpythia auet2bcteq6l1 dmv dm400 mm6000 w8pi qcut400
981 188495 madgraphpythia auet2bcteq6l1 dmv dm400 mm6000 w8pi qcut600
982 188484 madgraphpythia auet2bcteq6l1 dmv dm400 mm10000 w8pi qcut200
983 188490 madgraphpythia auet2bcteq6l1 dmv dm400 mm10000 w8pi qcut400
984 188496 madgraphpythia auet2bcteq6l1 dmv dm400 mm10000 w8pi qcut600
985 188485 madgraphpythia auet2bcteq6l1 dmv dm400 mm15000 w8pi qcut200
986 188491 madgraphpythia auet2bcteq6l1 dmv dm400 mm15000 w8pi qcut400
987 188497 madgraphpythia auet2bcteq6l1 dmv dm400 mm15000 w8pi qcut600

Bibliography

- [1] Collaboration ATLAS. Letter of Intent for the Phase-II Upgrade of the ATLAS Experiment. Dec 2012. URL <https://cds.cern.ch/record/1502664/>. Cited on pages 1, 17, 26, and 28.
- [2] B.H. Bransden and C.J. Joachain. *Quantum mechanics*. Pearson Education, second edition, 2000. Cited on page 3.
- [3] Sven-Patrik Hallsjö. Covering the sphere with noncontextuality inequalities. Bachelor's thesis, Linköping University, The Institute of Technology, 2013. URL [http://urn.kb.se/resolve?urn=urn:nbn:se:liu:diva-103663](http://urn.kb.se/resolve?urn=urn:nbn:se:liu.diva-103663). Cited on page 3.
- [4] A. Zee. *Quantum Field Theory in a Nutshell*. Princeton University Press, illustrated edition edition, March 2003. ISBN 0691010196. Cited on pages 3, 6, and 7.
- [5] Herbert Goldstein, Charles P. Poole, and John L. Safko. *Classical Mechanics (3rd Edition)*. Addison-Wesley, 3 edition, June 2001. ISBN 0201657023. Cited on page 3.
- [6] W. E. Burcham and M. Jobes. *Nuclear and Particle Physics*. Pearson education, second edition, 1995. Cited on page 4.
- [7] The ATLAS Collaboration. Observation of a new particle in the search for the Standard Model Higgs boson with the ATLAS detector at the LHC. *Phys. Lett. B*, 716(arXiv:1207.7214). CERN-PH-EP-2012-218):1–29. 39 p, Aug 2012. Cited on page 4.
- [8] Standard model of elementary particles. http://en.wikipedia.org/wiki/File:Standard_Model_of_Elementary_Particles.svg, 2014. Accessed: 2014-03-24. Cited on page 4.
- [9] G. Jungman, M. Kamionkowski, and K. Griest. Supersymmetric dark matter. *Physics Reports*, 267:195–373, March 1996. doi: 10.1016/0370-1573(95)00058-5. Cited on pages 4 and 5.

- 1017 [10] NASA. NASA's solar system exploration: the planets: orbits and
1018 physical characteristics. <https://solarsystem.nasa.gov/planets/>
1019 charchart.cfm, 2014. Accessed: 2014-03-21. Cited on page 6.
- 1020 [11] T. S. van Albada, J. N. Bahcall, K. Begeman, and R. Sancisi. Distribution
1021 of dark matter in the spiral galaxy NGC 3198. *Astrophysical Journal*, 295:
1022 305–313, August 1985. doi: 10.1086/163375. Cited on page 6.
- 1023 [12] Jessica Goodman, Masahiro Ibe, Arvind Rajaraman, William Shepherd,
1024 Tim M.P. Tait, et al. Constraints on Light Majorana dark Matter from Colliders.
1025 *Phys.Lett.*, B695:185–188, 2011. doi: 10.1016/j.physletb.2010.11.009.
1026 Cited on pages 5 and 7.
- 1027 [13] ATLAS Collaboration. Search for dark matter candidates and large extra di-
1028 mensions in events with a jet and missing transverse momentum with the at-
1029 las detector. *J. High Energy Phys.*, 04(arXiv:1210.4491. CERN-PH-EP-2012-
1030 210):075. 58 p, October 2012. URL [http://cds.cern.ch/record/](http://cds.cern.ch/record/1485031)
1031 1485031. Cited on pages 5, 8, and 9.
- 1032 [14] J. Goodman, M. Ibe, A. Rajaraman, W. Shepherd, T. M. P. Tait, and H.-B. Yu.
1033 Constraints on dark matter from colliders. *Phys.Rev.D82:116010,2010*, 82
1034 (11):116010, December 2010. doi: 10.1103/PhysRevD.82.116010. Cited on
1035 page 7.
- 1036 [15] ATLAS. Atlas luminosity public results. <https://twiki.cern.ch/twiki/bin/view/AtlasPublic/LuminosityPublicResults>, 2013.
1037 Accessed: 2014-03-06. Cited on page 10.
- 1038 [16] AC Team. The four main LHC experiments, Jun 1999. URL <http://cds.cern.ch/record/40525>. Cited on page 10.
- 1039 [17] Werner Herr and B Muratori. Concept of luminosity. 2006. URL <http://cds.cern.ch/record/941318/>. Cited on page 11.
- 1040 [18] The ATLAS Collaboration. The atlas experiment at the cern large hadron col-
1041 linder. *Journal of Instrumentation*, 3(08):S08003. 437 p, 2008. URL <https://cdsweb.cern.ch/record/1129811/>. Cited on pages 11 and 12.
- 1042 [19] Joao Pequenao. Computer generated image of the whole ATLAS detector,
1043 Mar 2008. URL <http://cds.cern.ch/record/1095924>. Cited on page
1044 12.
- 1045 [20] ATLAS Collaboration. Event display for one of the monojet candidates in
1046 the data. The event has a jet with $\text{pt} = 602 \text{ GeV}$ at $\eta = -1$ and $\phi =$
1047 2.6 , $\text{MET} = 523 \text{ GeV}$, and no additional jet with $\text{pt}_{\text{jet}} > 30 \text{ GeV}$ in the fi-
1048 nal state.. [https://atlas.web.cern.ch/Atlas/GROUPS/PHYSICS/](https://atlas.web.cern.ch/Atlas/GROUPS/PHYSICS/CONFNOTES/ATLAS-CONF-2011-096/fig_08.png)
1049 [CONFNOTES/ATLAS-CONF-2011-096/fig_08.png](https://atlas.web.cern.ch/Atlas/GROUPS/PHYSICS/CONFNOTES/ATLAS-CONF-2011-096/fig_08.png), 2011. Accessed:
1050 2014-03-28. Cited on page 13.
- 1051 [21] ATLAS Collaboration. Physics at a High-Luminosity LHC with ATLAS. Jul
1052

- 1056 2013. URL <https://cds.cern.ch/record/1564937>. Cited on page
1057 15.
- 1058 [22] J. Alwall, M. Herquet, F. Maltoni, O. Mattelaer, and T. Stelzer. MadGraph
1059 5: going beyond. *Journal of High Energy Physics*, 6:128, June 2011. doi:
1060 10.1007/JHEP06(2011)128. Cited on pages 15 and 33.
- 1061 [23] Torbjörn Sjöstrand, Stephen Mrenna, and Peter Skands. A brief introduc-
1062 tion to {PYTHIA} 8.1. *Computer Physics Communications*, 178(11):852 –
1063 867, 2008. ISSN 0010-4655. doi: [http://dx.doi.org/10.1016/j.cpc.2008.
1064 01.036](http://dx.doi.org/10.1016/j.cpc.2008.01.036). URL [http://www.sciencedirect.com/science/article/
1065 pii/S0010465508000441](http://www.sciencedirect.com/science/article/pii/S0010465508000441). Cited on pages 15 and 33.
- 1066 [24] The ROOT Team. Root. <http://root.cern.ch/drupal/>, 2014. Ac-
1067 cessed: 2014-03-28. Cited on page 15.
- 1068 [25] S. Agostinelli, J. Allison, K. Amako, J. Apostolakis, H. Araujo, P. Arce,
1069 M. Asai, D. Axen, S. Banerjee, G. Barrand, F. Behner, L. Bellagamba,
1070 J. Boudreau, L. Broglia, A. Brunengo, H. Burkhardt, S. Chauvie, J. Chuma,
1071 R. Chytracek, G. Cooperman, G. Cosmo, P. Degtyarenko, A. Dell'Acqua,
1072 G. Depaola, D. Dietrich, R. Enami, A. Feliciello, C. Ferguson, H. Fe-
1073 sefeldt, G. Folger, F. Foppiano, A. Forti, S. Garelli, S. Giani, R. Gi-
1074 annitrapani, D. Gibin, J.J. Gómez Cadenas, I. González, G. Gracia
1075 Abril, G. Greeniaus, W. Greiner, V. Grichine, A. Grossheim, S. Guatelli,
1076 P. Gumligner, R. Hamatsu, K. Hashimoto, H. Hasui, A. Heikkinen,
1077 A. Howard, V. Ivanchenko, A. Johnson, F.W. Jones, J. Kallenbach, N. Kanaya,
1078 M. Kawabata, Y. Kawabata, M. Kawaguti, S. Kelner, P. Kent, A. Kimura,
1079 T. Kodama, R. Kokoulin, M. Kossov, H. Kurashige, E. Lamanna, T. Lampén,
1080 V. Lara, V. Lefebure, F. Lei, M. Liendl, W. Lockman, F. Longo, S. Magni,
1081 M. Maire, E. Medernach, K. Minamimoto, P. Mora de Freitas, Y. Morita,
1082 K. Murakami, M. Nagamatu, R. Nartallo, P. Nieminen, T. Nishimura, K. Oht-
1083 subo, M. Okamura, S. O'Neale, Y. Oohata, K. Paech, J. Perl, A. Pfeiffer,
1084 M.G. Pia, F. Ranjard, A. Rybin, S. Sadilov, E. Di Salvo, G. Santin, T. Sasaki,
1085 N. Savvas, Y. Sawada, S. Scherer, S. Sei, V. Sirotenko, D. Smith, N. Starkov,
1086 H. Stoecker, J. Sulkimo, M. Takahata, S. Tanaka, E. Tcherniaev, E. Safai
1087 Tehrani, M. Tropeano, P. Truscott, H. Uno, L. Urban, P. Urban, M. Verderi,
1088 A. Walkden, W. Wander, H. Weber, J.P. Wellisch, T. Wenaus, D.C. Williams,
1089 D. Wright, T. Yamada, H. Yoshida, and D. Zschiesche. Geant4—a sim-
1090 ulation toolkit. *Nuclear Instruments and Methods in Physics Research*
1091 *Section A: Accelerators, Spectrometers, Detectors and Associated Equip-
1092 ment*, 506(3):250 – 303, 2003. ISSN 0168-9002. doi: [http://dx.doi.org/
1093 10.1016/S0168-9002\(03\)01368-8](http://dx.doi.org/10.1016/S0168-9002(03)01368-8). URL <http://www.sciencedirect.com/science/article/pii/S0168900203013688>. Cited on page 17.
- 1094 [26] ATLAS Collaboration. Performance assumptions for an upgraded ATLAS
1095 detector at a High-Luminosity LHC. Mar 2013. URL <https://cds.cern.ch/record/1527529/>. Cited on pages 17, 20, 26, 27, and 28.
- 1096 [27] ATLAS Collaboration. Electron performance measurements with the ATLAS
1097

1099 detector using the 2010 LHC proton-proton collision data. *Eur. Phys. J. C*,
1100 72(arXiv:1110.3174. CERN-PH-EP-2011-117):1909. 45 p, Oct 2011. Com-
1101 ments: 33 pages plus author list (45 pages total), 24 figures, 12 tables, sub-
1102 mitted to Eur. Phys. J. C. Cited on pages 26 and 28.

1103 [28] ATLAS Collaboration. Search for New Phenomena in Monojet plus Missing
1104 Transverse Momentum Final States using 10fb-1 of pp Collisions at $\sqrt{s}=8$
1105 TeV with the ATLAS detector at the LHC. Nov 2012. URL [http://cds.
1106 cern.ch/record/1493486/](http://cds.cern.ch/record/1493486/). Cited on pages 32, 33, 34, 36, and 37.

1107 [29] Donald Duck. The history of automatic control. *Duckburg Journal of Sci-
1108 ence*, 106(3):345–401, 2005. Cited on page 46.

1110 Upphovsrätt

1111 Detta dokument hålls tillgängligt på Internet — eller dess framtida ersättare —
 1112 under 25 år från publiceringsdatum under förutsättning att inga extraordinära
 1113 omständigheter uppstår.

1114 Tillgång till dokumentet innebär tillstånd för var och en att läsa, ladda ner,
 1115 skriva ut enstaka kopior för enskilt bruk och att använda det oförändrat för icke-
 1116 kommersiell forskning och för undervisning. Överföring av upphovsrätten vid
 1117 en senare tidpunkt kan inte upphäva detta tillstånd. All annan användning av
 1118 dokumentet kräver upphovsmannens medgivande. För att garantera äktheten,
 1119 säkerheten och tillgängligheten finns det lösningar av teknisk och administrativ
 1120 art.

1121 Upphovsmannens ideella rätt innehåller rätt att bli nämnd som upphovsman
 1122 i den omfattning som god sed kräver vid användning av dokumentet på ovan
 1123 beskrivna sätt samt skydd mot att dokumentet ändras eller presenteras i sådan
 1124 form eller i sådant sammanhang som är kränkande för upphovsmannens litterära
 1125 eller konstnärliga anseende eller egenart.

1126 För ytterligare information om Linköping University Electronic Press se för-
 1127 lagets hemsida <http://www.ep.liu.se/>

1128 Copyright

1129 The publishers will keep this document online on the Internet — or its possi-
 1130 ble replacement — for a period of 25 years from the date of publication barring
 1131 exceptional circumstances.

1132 The online availability of the document implies a permanent permission for
 1133 anyone to read, to download, to print out single copies for his/her own use and
 1134 to use it unchanged for any non-commercial research and educational purpose.
 1135 Subsequent transfers of copyright cannot revoke this permission. All other uses
 1136 of the document are conditional on the consent of the copyright owner. The
 1137 publisher has taken technical and administrative measures to assure authenticity,
 1138 security and accessibility.

1139 According to intellectual property law the author has the right to be men-
 1140 tioned when his/her work is accessed as described above and to be protected
 1141 against infringement.

1142 For additional information about the Linköping University Electronic Press
 1143 and its procedures for publication and for assurance of document integrity, please
 1144 refer to its www home page: <http://www.ep.liu.se/>